The Wintertime Southern Hemisphere Split Jet: Structure, Variability, and Evolution

TERESA M. BALS-ELSHOLZ, EYAD H. ATALLAH, LANCE F. BOSART, THOMAS A. WASULA,* MICHAEL J. CEMPA,* AND ANTHONY R. LUPO+

Department of Earth and Atmospheric Sciences, University at Albany, State University of New York, Albany, New York

(Manuscript received 5 December 2000, in final form 8 May 2001)

ABSTRACT

A persistent feature of the Southern Hemisphere upper-level time-mean flow is the presence of a split jet across the South Pacific east of Australia during the austral winter. The split jet is composed of the subtropical jet (STJ) on its equatorward branch and the polar front jet (PFJ) on its poleward branch. The NCEP–NCAR reanalysis is used to investigate the structure and evolution of the split jet. Results show that the presence/absence of the PFJ determines the degree of split flow, given that the STJ is a quasi-steady feature. A split-flow index (SFI) is developed to quantify the variability of the split jet, in which negative values represent strong split flow and positive values nonsplit flow. Correlations with teleconnection indices are investigated, with the SFI positively correlated to the Southern Oscillation index and negatively correlated to the Antarctic oscillation.

The SFI is used to construct composites of heights, temperature, and wind for split-flow and non-split-flow days. The composites reveal that relatively cold conditions occur in the South Pacific in association with non-split-flow regimes, and split-flow regimes occur when relatively warm conditions prevail. In the latter situation cold air bottled up over Antarctica helps to augment the background tropospheric thickness gradient between Antarctica and the lower latitudes with a resulting increase in the thermal wind and the PFJ. It is surmised that frequent cold surges out of Antarctica moving into the South Pacific are associated with non-split-flow regimes. In this context, the variability of the split jet responds to large-scale baroclinic processes and is further modulated by synoptic-scale disturbances.

1. Introduction

A distinct characteristic of the climatological time-mean flow during winter in the Southern Hemisphere (SH) is the presence of a split jet at the longitudes of Australia and New Zealand. The equatorward branch of the time-mean split jet is anchored by a strong subtropical jet (STJ) that extends eastward between 25° and 30°S from the central South Indian Ocean across Australia to the east-central South Pacific Ocean near 130°W. A zone of weak westerlies lies poleward of the STJ from southeastern Australia eastward across the South Island of New Zealand to east of the date line. The poleward branch of the time-mean split jet is anchored by the polar front jet (PFJ). The PFJ is concentrated along 60°S from 140°E to 150°W. The existence of the winter time-mean split jet in the SH has been well documented (see, e.g., Taljaard 1972; van Loon 1972a,b,c; Hurrell et al. 1998; van Heerden and Taljaard 1998; Vincent and Silva Dias 1998).

Taljaard (1972, his Fig. 8.45) suggested that the location, existence, and strength of the SH split jet in winter was strongly influenced by relative cooling over the Australian landmass and outflow from the great Asiatic summer monsoon anticyclone of the Northern Hemisphere (NH) into the SH at the longitudes of Australia. Enhanced cooling over the southern half of Australia as compared to the adjacent oceans in winter results in increased baroclinicity over southern Australia relative to the ocean waters south of Australia, effectively shifting the primary cool season thermal gradient equatorward (see also Hurrell et al. 1998, their Figs. 1.1 and 1.3). Meanwhile, a secondary baroclinic zone can be found farther poleward near 60°S close to the edge of the Antarctic pack ice. Cross-equatorial flow from the NH to the SH during the SH winter, at the longitudes of Australia (see, e.g., Newton 1972; Hurrell et al. 1998), may also contribute to the intensity of the STJ in the SH via Coriolis torques and through a strengthening of the tropical meridional temperature gradient due to subsidence in conjunction with the time-mean Hadley circulation.

* Current affiliation: National Weather Service, Albany, New York.
+ Current affiliation: University of Missouri—Columbia, Columbia, Missouri.

Corresponding author address: Teresa M. Bals-Elsholz, Department of Earth and Atmospheric Sciences, University at Albany, State University of New York, 1400 Washington Avenue, Albany, NY 12222.
E-mail: teresa@atmos.albany.edu

Blocking has also been shown to play a role in the modulation of the intensity of the SH split jet (e.g., Trenberth and Mo 1985; Mo et al. 1987; Trenberth 1986b, 1991). An early study by van Loon (1956) demonstrated that blocking in the SH winter was favored in the southwest Pacific Ocean and to the southeast of Australia. More recent studies (e.g., Marques and Rao 1999; Renwick and Revell 1999) have confirmed the earlier findings and have established that the area near South America is an important secondary blocking region in winter and spring. Vincent (1994), Vincent et al. (1997), and Vincent and Silva Dias (1998) have further demonstrated that the location and intensity of the midlatitude portion of the South Pacific convergence zone (SPCZ) is modulated by jet streaks associated with the STJ that in turn modulate cyclone activity along the SPCZ. Blocking activity in the Australia–New Zealand sector can be also modulated by jet streaks and cyclonic activity along the SPCZ through the enhancement of midlatitude anticyclones via poleward eddy heat and vorticity fluxes, especially when the SPCZ is displaced westward from its usual position (e.g., Kidson and Sinclair 1995). Other potentially important aspects of the SH split jet in winter would include cold air outbreaks associated with high-latitude blocking activity (e.g., Mo et al. 1987), the breakdown of the Antarctic polar vortex in late spring (e.g., Mechoso et al. 1988), Rossby wave forcing (e.g., James 1988), and the phase of the El Niño–Southern Oscillation (e.g., Karoly 1989; Chen et al. 1996).

Common to most of these studies has been an emphasis on documenting and understanding the time-mean flow signatures on intraseasonal and seasonal timescales. The purpose of this study is to examine the structure and evolution of the winter season SH split jet. We will develop a split-flow index (SFI) to quantify the magnitude of the split flow and we will use the SFI to examine the variability of the split jet on intraseasonal and interannual timescales and to construct composites of split-flow and non-split-flow regimes so as to better understand the life cycle of the SH split jet. In particular, we will show that the existence of the split jet is highly dependent upon the presence/absence of the PFJ, given that the STJ is a quasi-permanent feature of the SH winter season. Our analysis is facilitated by the availability of a 43-yr reanalysis dataset provided by the National Centers for Environmental Prediction (NCEP) and the National Center for Atmospheric Research (NCAR; see Kalnay et al. 1996; Kistler et al. 2001). The paper is organized as follows. The methodology is enumerated in section 2 and the SFI is formally defined in section 3. The climatology and synoptic setting of split-flow and non-split-flow regimes are discussed in section 4, section 5 places the flow regime in terms of the thermal structure and low-level heights, and the concluding discussion appears in section 6.

2. Data and methodology

The NCEP–NCAR reanalysis (hereinafter referred to as the reanalysis) was used to examine the SH split jet. This global dataset is on a 2.5° latitude–longitude grid with data coverage at the time of writing from 1 January 1948 to 31 December 2000. The gridded data were stored, analyzed, and displayed using the General Meteorological Package (GEMPAK; Koch et al. 1983).

The reanalysis data in the SH contain improperly ingested PAOBS data (bogused sea level pressures) for the time period 1979–92.[1] The impact of the error is felt mostly at low levels in the SH high and midlatitudes (poleward of 40°S) during the cool season. For this reason, the years 1979–92 are not included in the synoptic-scale composite studies. Data above 500 hPa are less affected. Monthly data at all levels show negligible effects from the PAOBS problem.

Kistler et al. (2001) advise that the reanalysis prior to the International Geophysical Year (IGY) is intended for NH use only. Monthly and seasonal climatologies were computed from the reanalysis monthly means for the time period of the IGY, 1958–2000. Hines et al. (2000) caution on the use of the reanalysis in the SH prior to 1970 due to long-term reductions in surface pressure. After examining the winter zonal wind in the reanalysis from the IGY through 2000, we felt that the split jet was adequately represented by the reanalysis prior to 1970. Linear trends for two time periods are presented in sections 3 and 4 and in Table 4.

Since the three austral winter months of July, August, and September had the most pronounced split jet, the seasonal climatology was broken into 3-month seasons of January–February–March (JFM); April–May–June (AMJ); July–August–September (JAS); and October–November–December (OND). The monthly data were averaged to create the seasonal climatologies.

In order to investigate aspects of the global circulation at low latitudes, as well as high latitudes, our analysis of the SH began with the reanalysis monthly streamfunction (ψ) and velocity potential (ϕ). The magnitude of the nondivergent wind ($|\mathbf{V}_{ND}|$) was derived from the streamfunction, where $|\mathbf{V}_{ND}| = |\hat{k} \times \nabla\psi|$. The relative vorticity (ζ) was also derived from the streamfunction, where $\zeta = \nabla \cdot \nabla\psi$. The divergent wind ($\mathbf{V}_D$) was derived from the velocity potential, where $\mathbf{V}_D = \nabla\phi$ and $\nabla \cdot \mathbf{V}_D = \nabla \cdot \nabla\Phi$. The daily streamfunction grids were not initially available from the reanalysis for the computation of the relative vorticity in the composite study in section 4, therefore the relative vorticity for the daily grids was derived from the horizontal wind, where $\zeta = \hat{k} \cdot \nabla \times \mathbf{V}$. Monthly relative vorticity was recomputed from the daily wind grids and compared with the monthly relative

[1] Full details on the PAOBS problem and diagnostic studies by the Climate Prediction Center on the effect of the incorrect PAOBS on the reanalysis can be found online at http://wesley.wwb.noaa.gov/paobs/paobs.html.

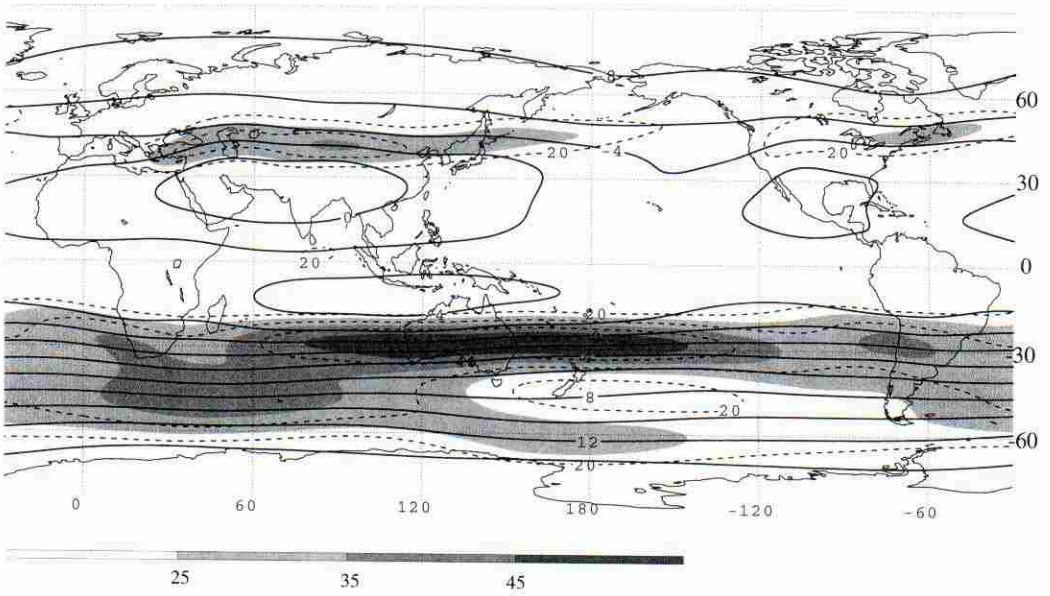

FIG. 1. Climatology of the upper-level flow at 200 hPa for JAS 1958–2000. Streamfunction contoured (solid) every 2×10^7 m^2 s^{-1} and isotachs, derived from the streamfunction, contoured (dashed) every 10 m s^{-1} starting at 20 m s^{-1}, shaded every 10 m s^{-1} above 25 m s^{-1}.

vorticity derived from the streamfunction. The two fields were found to be in very close agreement, with a 0.99 correlation significant at the 99.9% level. Daily velocity potential and streamfunction values for the composites were computed from the 17 levels of the daily reanalysis winds.

Correlation coefficients were calculated between various teleconnection indices and seasonal areal averages of the split jet from 1958 to 2000. Therefore, the number of observations (yr) or degrees of freedom used for the correlations is 43 ($n = 43$), except for the Antarctic oscillation and annual lagged correlations, where $n = 42$ for 1958–99 data. The correlations calculated are Pearson correlations (Panofsky and Brier 1958; Wilks 1995). Significance of the correlations is tested by applying one- and two-tailed tests (Powell 1982).

3. Split-flow index

The SH time-mean flow for JAS at 200 hPa (Fig. 1) clearly displays the split-jet feature across the South Pacific. The STJ, stretching from the south Indian Ocean across the South Pacific Ocean, is paralleled in the South Pacific Ocean by a weaker jet, the PFJ, with a distinct minimum in the westerlies between the two jets. The SH split jet varies little in location from year to year, but does vary greatly in magnitude. In order to quantify these variations in the magnitude of the split jet, Hovmöller plots of the zonal wind were created for the 43 yr of the reanalysis. In Fig. 2a the climatological JAS zonal wind at 200 hPa is contoured for the SH. Note that the zonal wind and the magnitude of the nondivergent wind in Fig. 1 are in close agreement, especially in the area of the split jet. Figure 3 shows a 10-yr (1990–99) Hovmöller plot of the zonal wind from 80°S to the equator averaged across 160°E–160°W. The split jet is centered at this longitude, and the 10 yr selected are representative of the variations in the split jet. The STJ is readily apparent each austral autumn through spring between 25° and 30°S. Following the STJ onset, the peak magnitude of the PFJ between 55° and 60°S generally occurs in July or August. The majority of the winters displayed show distinct PFJ maxima. The PFJ region in 1991 and 1992 exhibits no distinct wind maximum above 30 m s^{-1}. In addition, it is difficult to define an area where the minimum in westerly velocities between the STJ and PFJ was located for these two years.

In Fig. 2b, the climatology of the relative vorticity derived from the reanalysis streamfunction is shown for the SH. Two maxima of anticyclonic relative vorticity (positive in the SH) lie equatorward of the STJ across the south Indian Ocean and the western South Pacific Ocean. Poleward of the STJ the cyclonic vorticity maximum stretches across Australia and over the western South Pacific. The anticyclonic and cyclonic relative vorticity couplet of the PFJ in the South Pacific is smaller in magnitude than the STJ couplet, as expected from the weaker PFJ, but is still distinct.

A Hovmöller plot of the derived relative vorticity is displayed in Fig. 4 for the same 10-yr period as Fig. 3. As in Figs. 2 and 3, the STJ stands out clearly, with the anticyclonic relative vorticity equatorward of the STJ being the dominant feature. In addition, the wintertime PFJ is clearly indicated by the cyclonic relative vorticity poleward of the PFJ between 55° and 60°S. The STJ cyclonic relative vorticity (poleward of the winter STJ)

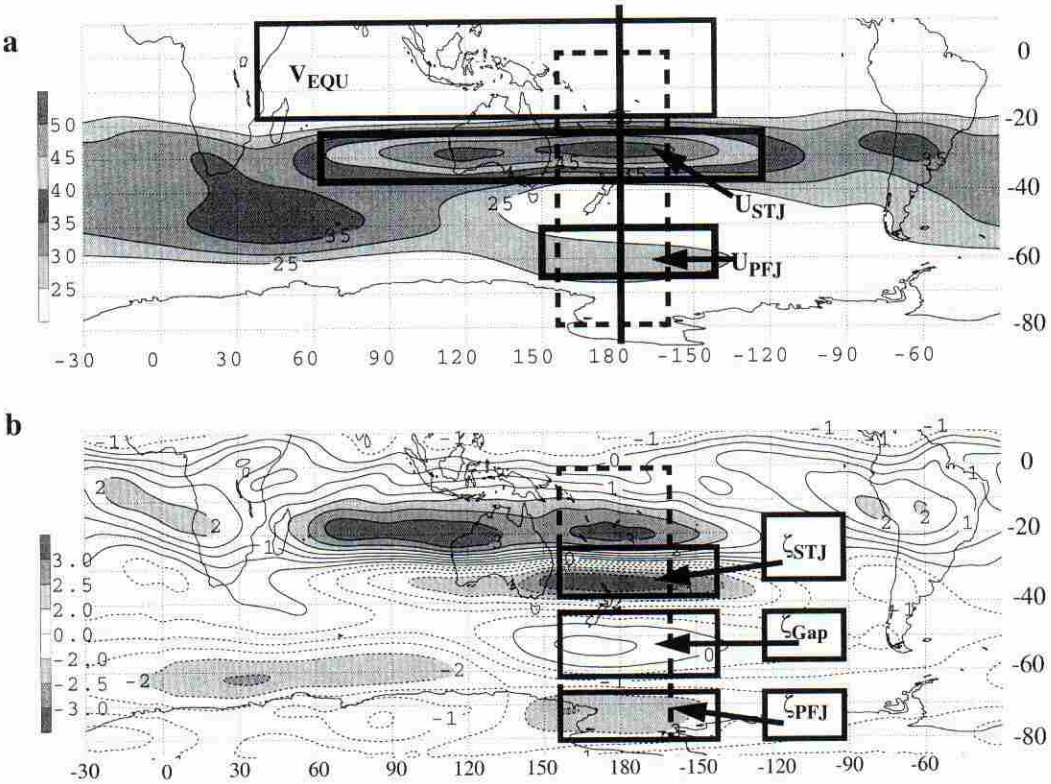

FIG. 2. The zonal wind and relative vorticity, derived from the streamfunction, for the 200-hPa JAS climatology in the Southern Hemisphere. (a) The zonal wind is shaded every 5 m s^{-1} above 25 m s^{-1}, boxes for correlation calculations in Table 2 are outlined, and the solid line at the date line indicates the region for vertical cross sections in Figs. 19 and 20. (b) Anticyclonic (cyclonic) relative vorticity isopleths are the solid (dashed) contours every 0.5 $\times$ 10^{-5} s^{-1} and shaded for values greater than 2 $\times$ 10^{-5} s^{-1}, boxes for computations of the split-flow index are outlined and labeled. Boxes for the Hovmöller plots in Figs. 3 and 4 are outlined by a dashed line in both figures.

has slightly weaker magnitude values than the STJ anticyclonic relative vorticity. In contrast, the PFJ anticyclonic relative vorticity (equatorward of the PFJ) is much weaker in magnitude than the PFJ cyclonic relative vorticity, with only small areas of positive relative vorticity. The overlap in area of the STJ cyclonic relative vorticity with the PFJ anticyclonic relative vorticity results in weaker values. This overlap is the region of the minimum in the westerlies between the two jets.

a. Definition of the split-flow index

After an examination of Hovmöller plots for 43 yr of derived relative vorticity, a strategy for quantifying the split flow was devised. Three regions best defined the split jet: the PFJ, the STJ, and the minimum between the two jets. Area averages of the relative vorticity across three locations for the winter season (JAS) split jet between 160°E and 140°W (Fig. 2b) were calculated: the cyclonic side of the PFJ from 65° to 77.5°S (ζ_{PFJ}); the anticyclonic side of the PFJ from 40° to 57.5°S (ζ_{Gap}); and, in order to reduce the relative magnitude of the STJ component, but not disregard its influence, a region crossing the gradient of the cyclonic and anticyclonic vorticity of the STJ from 25° to 35°S (ζ_{STJ}). The cyclonic vorticity average of ζ_{PFJ} and the gradient average of ζ_{STJ} were summed and the anticyclonic vorticity average of ζ_{Gap}, which is positive for strongly split flow, was subtracted from the sum to create the SFI:

$$\zeta_{PFJ} + \zeta_{STJ} - \zeta_{Gap} = \text{SFI}.$$

The SFI was normalized by subtracting the 43-yr mean from each year's SFI value and dividing the result by the 43-yr standard deviation.

Time series of each SFI component are shown in Fig. 5a, and a normalized time series of the SFI is shown in Fig. 5b. Years with a split-flow regime similar to the climatological mean have normalized SFI values near zero, as in 1971, 1978, and 1996. Years with pronounced split flow such as 1984, 1989, and 1997 have a strong PFJ with relatively high cyclonic vorticity, and a higher PFJ anticyclonic vorticity in the velocity minimum between the STJ and PFJ, resulting in a large negative value of the SFI. Years with a weak or no split jet, such as 1964, 1980, and 1981, have a weak or nonexistent PFJ, the anticyclonic region between the STJ and climatological PFJ is reduced in area and becomes more cyclonic, and the SFI is more positive. The 43-yr linear

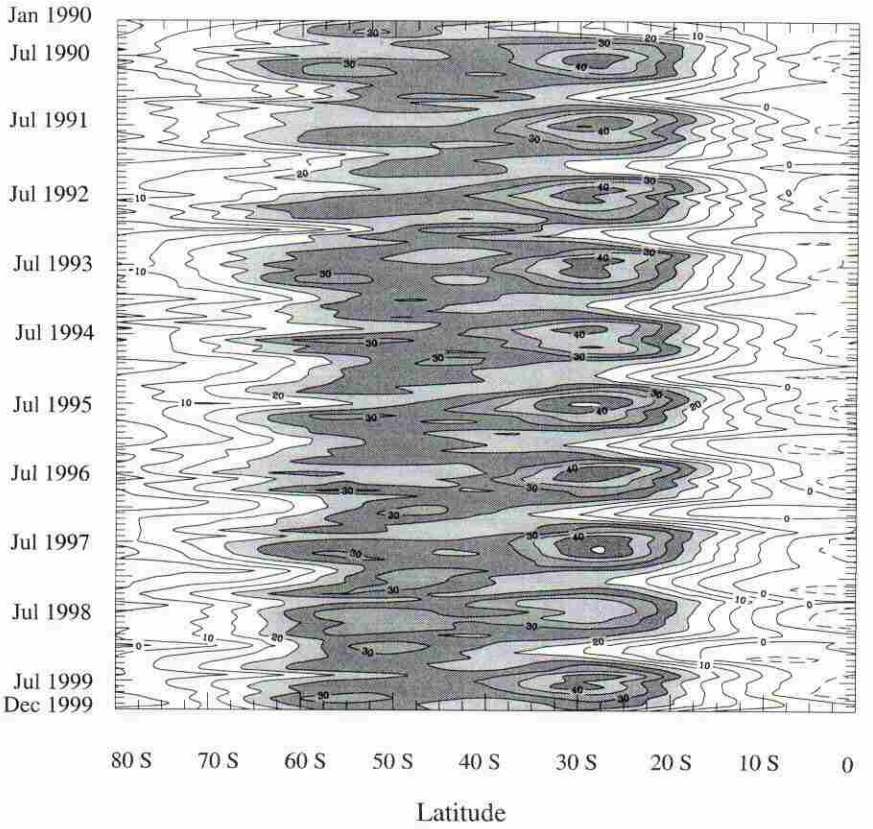

FIG. 3. Hovmöller plot of the monthly zonal wind isotachs from Jan 1990 to Dec 1999 averaged between 160°E and 160°W from the equator to 80°S. Isotachs are contoured every 5 m s^{-1} with values above 20 m s^{-1} shaded; solid (dashed) contours are westerly (easterly).

trends for the SFI components and the SFI revealed that ζ_{PFJ} and ζ_{Gap} had slopes of 1.1×10^{-4} and -0.4×10^{-4} s^{-1} yr^{-1} and standard deviations of 3.3×10^{-2} and 2.6×10^{-2} s^{-1} yr^{-1}, respectively, while ζ_{STJ} and the SFI increased slightly with time at 2.8×10^{-4} and 4.3×10^{-4} s^{-1} yr^{-1}, respectively, and standard deviations of 3.9×10^{-2} s^{-1} yr^{-1} for ζ_{STJ} and 7.8×10^{-2} s^{-1} yr^{-1} for the SFI.

b. Correlations

As both an objective check of the SFI and as a method to understand how the components of the SFI relate to each other over the period of the climatology, correlations were computed between the individual SFI components and the SFI (Table 1). Each component contributes significantly to the SFI, however, ζ_{PFJ} and ζ_{Gap} contribute the most, 0.80 and -0.83, respectively, while ζ_{STJ} has a correlation of 0.75. The negative correlation of ζ_{Gap} with the SFI underscores the increased anticyclonic vorticity present in the gap region during split-flow years. The dependence of ζ_{PFJ} and ζ_{Gap} on each other is denoted by their correlation of -0.68. The ζ_{STJ} reflects its contribution to ζ_{Gap} with a correlation of -0.40. The ζ_{STJ} has a small, though still significant at the 95% level, correlation to ζ_{PFJ} with a value of 0.28.

In order to determine whether the SFI is modulated by other global phenomena, correlations were computed between the SFI, teleconnection indices, and global circulation features. Little correlation was found between the North Atlantic oscillation (Hurrell 1995) and the SFI (not shown), but, not surprisingly, the Southern Oscillation index (SOI), the Antarctic oscillation (AAO; Thompson and Wallace 2000), and the Pacific decadal oscillation (PDO; Mantua et al. 1997) had significant correlations with features of the split flow. Table 2 contains correlations between the SFI, the SOI, the AAO, the PDO, the zonal wind in the STJ (U_{STJ}) averaged across the south Indian Ocean and South Pacific from 70°E to 130°W and 25° to 35°S, the zonal wind of the PFJ (U_{PFJ}) in the South Pacific averaged from 150°E to 150°W and 55° to 65°S, and the cross-equatorial flow in the Indian Ocean (V_{EQU}) averaged from 40°E to 140°W and 20°S to 10°N. The areas where the correlations were calculated are outlined by the boxes in Fig. 2a.

The correlation between the zonal wind of the jets highlights the dependence of the SFI on the presence of the PFJ. The U_{PFJ} and the SFI had a high correlation at -0.77 (significant at the 99.9% level), while the correlation of U_{STJ} to the SFI was significant (97.5%) but

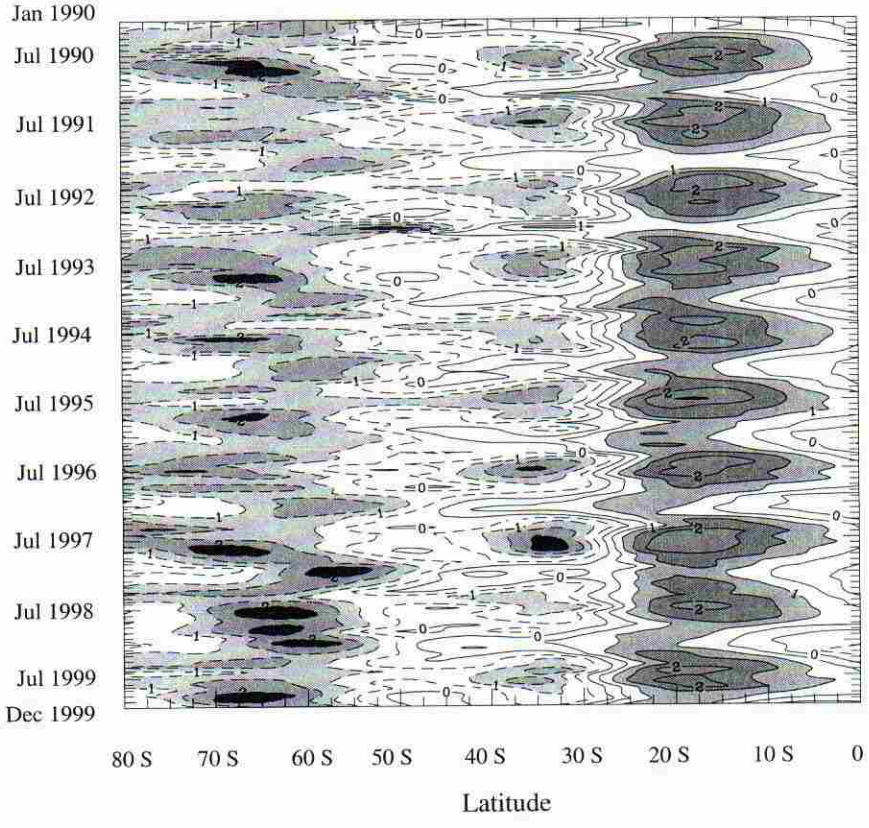

FIG. 4. Hovmöller plot of the monthly relative vorticity from Jan 1990 to Dec 1999 averaged between 160°E and 160°W from the equator to 80°S. Anticyclonic (cyclonic) relative vorticity isopleths are solid (dashed) every 0.5×10^{-5} s^{-1} and are shaded above 1×10^{-5} s^{-1}.

low at -0.31. A strong PFJ results in a low SFI value, reiterating the SFI definition, but a variation in the STJ strength does not necessarily correlate to a particular SFI phase. The correlation between the SFI and V_{EQU}, though significant at the 99.0% level, was fairly low at 0.37 and is most likely due to the influence of the STJ, where V_{EQU} and U_{STJ} had a correlation of -0.51 significant at the 99.9% level.

The SFI and the SOI had a low correlation of 0.33, significant at the 97.5% level. A slightly more meaningful relationship can be drawn from U_{STJ} and the SOI where a correlation coefficient of -0.41 (99.5%) was found. A series of lagged SOI correlations to the SFI and to the jets was also computed, stepping back month-by-month from JAS to January, to 1 yr prior to the SFI, and to 1 yr after the SFI (Table 3). By far the largest correlations, for all but the U_{PFJ}, occurred during the same season (see SOI for JAS in Table 2) as the SFI computation. The SFI correlation dropped to zero, while U_{PFJ} increased to its high of a 0.14 correlation with the SOI in the March–April–May 3-month period. The U_{STJ} reversed sign in February-March-April. The V_{EQU} decreased steadily with time. Correlations with the SOI 1 yr prior and 1 yr later were also lower and less significant than the correlations to the SOI of the same season. Chen et al. (1996) looked at the zonal wind in the jets from 180° to 120°W in comparison with the 1987 SOI minimum and the 1989 SOI maximum. They found a strong STJ and weak PFJ the year before the SOI minimum and a dramatically weaker STJ and a strong PFJ the year before the SOI maximum. Our correlations across the climatology, using both our zonal wind areas and the Chen et al. (1996) areas, were not significant enough to draw a profound connection between the SOI and the split-flow regime or the PFJ.

In Table 2 a strong correlation was established between V_{EQU} and SOI with a correlation of 0.87 (99.9%). Outflow from the Asian anticyclone crosses the equator over the Indian Ocean and western South Pacific and is torqued by the Coriolis force in the SH into westerly flow. This westerly flow has a positive impact on the strength of the STJ as described by Newton (1972) and Hurrell et al. (1998). A positive (negative) SOI, or La Niña (El Niño), favors weaker (stronger) cross-equatorial flow and decreased (increased) westerlies in the STJ. No significant relationship was established between the V_{EQU} and U_{PFJ}, (0.02), nor between U_{PFJ} and the SOI (0.01), indicating that the influence of the Asian anticyclone did not extend to the high latitudes of the

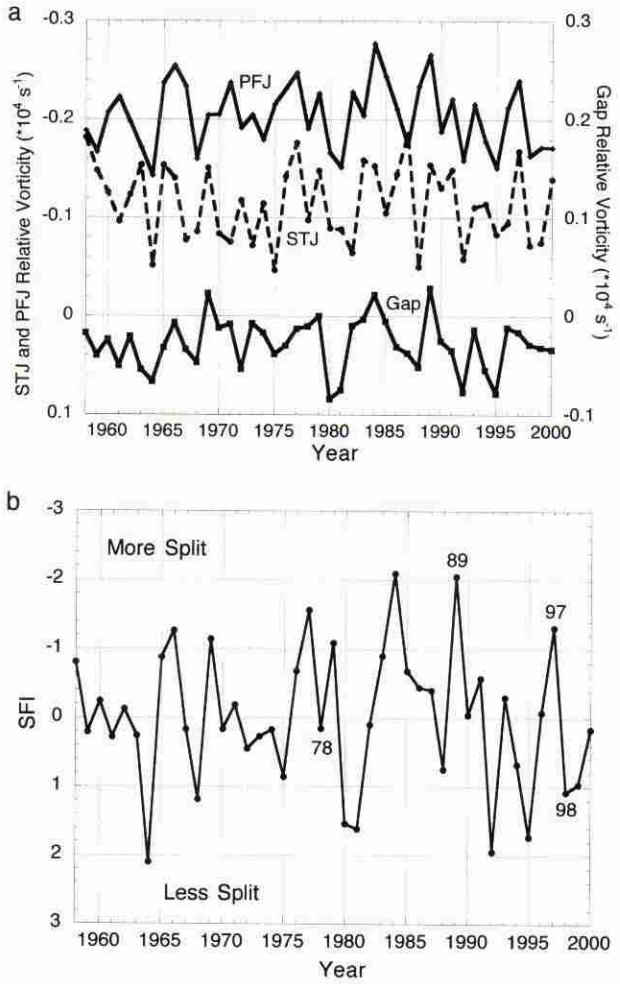

FIG. 5. Time series (1958–2000) of (a) the individual components of the SFI and (b) the normalized SFI.

PFJ in this region and season and is reflected in the low correlation of the SFI and SOI.

The North Pacific Ocean measure of SST anomalies, the PDO had a significant correlation to the SOI and to V_{EQU}. The impact of decadal oscillations of the North Pacific had little impact on the phase of the split flow, the SFI had a small correlation of -0.23, which just missed the first significance level of 95%. Neither U_{STJ} nor U_{PFJ} had any significant correlation to the PDO. The SFI and the AAO had a negative correlation of -0.32 (97.5%) and U_{STJ} had a more significant correlation at -0.48 (99.5%). The higher-latitude U_{PFJ} was strongly correlated with the AAO at 0.68 (99.9%), reflecting the response of the PFJ to the positive 850-hPa height anomalies at high latitudes in a positive AAO. The high-latitude annular mode expressed by the AAO made its impact on the PFJ, and thus to a lesser extent the SFI, in much the same measure as the tropical SOI has on the STJ, and again to a lesser extent to the SFI.

TABLE 1. Correlation and significance values of the SFI and its components.

	SFI	ζ_{STJ}	ζ_{Gap}	ζ_{PFJ}
SFI	—	0.75 (99.9%)	−0.83 (99.9%)	0.80 (99.9%)
ζ_{STJ}	0.75 (99.9%)	—	−0.40 (99.5%)	0.28 (95.0%)
ζ_{Gap}	−0.83 (99.9%)	−0.40 (99.5%)	—	−0.68 (99.9%)
ζ_{PFJ}	0.80 (99.9%)	0.28 (95.0%)	−0.68 (99.9%)	—

4. Split-flow climatology, composites, and anomalies

In this section we will examine the SH split flow in the context of the seasonal and global climatology. The representativeness of the SFI will be examined through examples of the JAS upper-level flow for individual years. The evolution and dissipation of the split flow will be presented through composites of split-flow and non-split-flow events.

a. Streamfunction seasonal climatology

The development of the SH split jet can be seen in the seasonal climatologies of the streamfunction. In austral summer (Fig. 6a) the global climatology at 200 hPa is dominated by the NH jet over the western Pacific. A large anticyclone resides just north of the equator over Africa eastward across the Indian Ocean into the west Pacific. In the SH, the PFJ lies over the eastern South Pacific eastward across the South Atlantic and Indian Oceans to near the date line. The PFJ bulges equatorward near the continental landmasses in response to the strong thermal gradient between the cold oceans and warm continents. No sign of split flow occurs over the western South Pacific during this season. During austral fall (Fig. 6b), the STJ begins to develop across the Indian Ocean, Australia, and the Pacific Ocean. The anticyclone diminishes over the NH, while an anticyclone develops over the south Indian Ocean between western Australia and Indonesia. The PFJ persists along the intense thermal gradient between the cold Antarctic and the warm African landmass. The PFJ continues eastward across the south Indian Ocean to south of Australia, signaling the onset of the split flow in the south Tasman Sea.

By austral winter (Fig. 1) the STJ, PFJ, and resulting split flow are firmly in place across the South Pacific. Two separate wind maxima at 200 hPa can be seen, one anchored over southwest Australia, with the other centered equatorward of New Zealand. The NH summer anticyclone is centered over India, while the SH anticyclone remains over the south Indian Ocean and stretches eastward across the Coral Sea into the South Pacific. The region of split flow stretches from 135°E to 140°W. By austral spring (Fig. 6c), the region of split

TABLE 2. Correlation and significance values of the SFI, SOI, AAO, PDO, 200-hPa zonal winds of the STJ and PFJ, and 200-hPa cross-equatorial winds for JAS.

	SFI	U_{STJ}	U_{PFJ}	V_{EQU}	SOI	AAO	PDO
SFI	—	−0.31 (97.5%)	−0.77 (99.9%)	0.37 (99.0%)	0.33 (97.5%)	−0.32 (97.5%)	−0.23 (<95%)
U_{STJ}	−0.31 (97.5%)	—	−0.14	−0.51 (99.9%)	−0.41 (99.5%)	−0.48 (99.5%)	0.09
U_{PFJ}	−0.77 (99.9%)	−0.14	—	0.02	0.01	0.68 (99.9%)	0.09
V_{EQU}	0.37 (99.0%)	0.51 (99.9%)	0.02	—	0.87 (99.9%)	−0.07	−0.60 (99.9%)
SOI	0.33 (97.5%)	−0.41 (99.5%)	0.01	0.87 (99.9%)	—	−0.07	−0.44 (99.5%)
AAO	−0.32 (97.5%)	−0.48 (99.5%)	0.68 (99.9%)	−0.07	−0.07	—	0.30 (95%)
PDO	−0.23 (<95%)	0.09	0.09	−0.60 (99.9%)	−0.44 (99.5%)	0.30 (95%)	—

flow has decreased in area, although a minimum still exists between the two weakened jets. In the SH the anticyclone has diminished. The NH anticyclone has shifted equatorward over the relatively warm waters of the Indian Ocean and the west Pacific.

b. *Annual split-flow streamfunction variability*

In Fig. 5b, the variability of the split flow was apparent in the wide swings between the extremes of no-split and enhanced-split years. A subjective check of the SFI for the JAS split flow was made for each year of the reanalysis. Every year, with only one exception, was accurately categorized by its SFI value. Three years with contrasting SFI values are shown in Fig. 7. In 1978 (Fig. 7a) with a near-normal SFI at 0.2 SFI, the 200-hPa PFJ was clearly separate from and parallel to the STJ across the south Indian Ocean and the South Pacific. The STJ stretched across the Indian Ocean and Australia, but was weaker than climatology across the western Pacific and South America. In the strongly split year (−2.0 SFI) of 1989 (Fig. 7b), a broad area of minimum in the velocity field delineating the split flow was centered on the date line in the South Pacific with the PFJ stretching from near 120°E to 120°W. Across the south Indian Ocean, the PFJ was slightly stronger and the STJ was much weaker than in 1978. The large positive SFI (1.5 SFI) of 1980 (Fig. 7c) was characterized by a single jet. The PFJ extended from the South Atlantic across the south Indian Ocean and then appeared to merge with the STJ west of Australia. The STJ was the sole feature across the South Pacific.

In each of the examples shown, the SFI objectively described the degree of split in the South Pacific flow. The SFI accurately categorized the split flow for the entire time series of the reanalysis with the exception of 1998. In 1998 (Fig. 8b) a distinct STJ and PFJ, characteristic of split flow, were centered over New Zealand. However, the SFI ranked 1998 as a low split year with a value of 1.1, which can be compared with 1975 (Fig. 8a) with a SFI value of 0.9, and to 1999 (Fig. 8c) with an SFI of 1.0. The 1975 winter season had a weak PFJ stretching to 140°W. The 1999 PFJ was stronger, but stretched to only 175°W. The 1998 PFJ was neither missing nor weaker than climatology; in fact the PFJ was rather robust with a 30 m s^{-1} isotach nearly the width of the Pacific Ocean. However, the 1998 STJ in the South Pacific was dramatically weaker than normal. Averaged across the area of the split flow in the South Pacific (box U_{STJ} in Fig. 2a and plotted in Fig. 9), the 1998 STJ was the weakest STJ in 43 yr, The STJ of 1999, with a more representative SFI of 1.0, was the second weakest.

The anomalous minimum in the average zonal wind of the STJ in 1998 is responsible for the one instance in the 43-yr climatology where our objective definition of the split flow, as given by the SFI, fails to agree with a subjective analysis of the flow regime. This failure arises from the small magnitude of the relative vorticity associated with the STJ in 1998 (Fig. 5a), leading to a normalized SFI value of 1.1. Since the STJ is a key component of the SFI (Table 1) and a fairly steady feature of the SH flow pattern (Fig. 5a), the anomalous behavior of the STJ had a large impact on the SFI. We attempted to refine the SFI to better describe 1998, by redefining the areas of calculations, by using different

TABLE 3. SOI lag correlations to JAS values for 3-month periods before JAS and for 1 yr before (−1) and 1 yr after (+1) JAS.

	JFM	FMA	MAM	AMJ	MJJ	JJA	SOI − 1	SOI + 1
SFI	−0.08	−0.09	0.00	0.10	0.22	0.31	−0.14	−0.15
U_{STJ}	0.12	0.09	−0.06	−0.18	−0.32	−0.35	0.22	0.17
U_{PFJ}	0.03	0.10	0.14	0.11	0.06	0.01	0.01	0.01
V_{EQU}	0.11	0.27	0.51	0.62	0.67	0.78	−0.14	−0.03

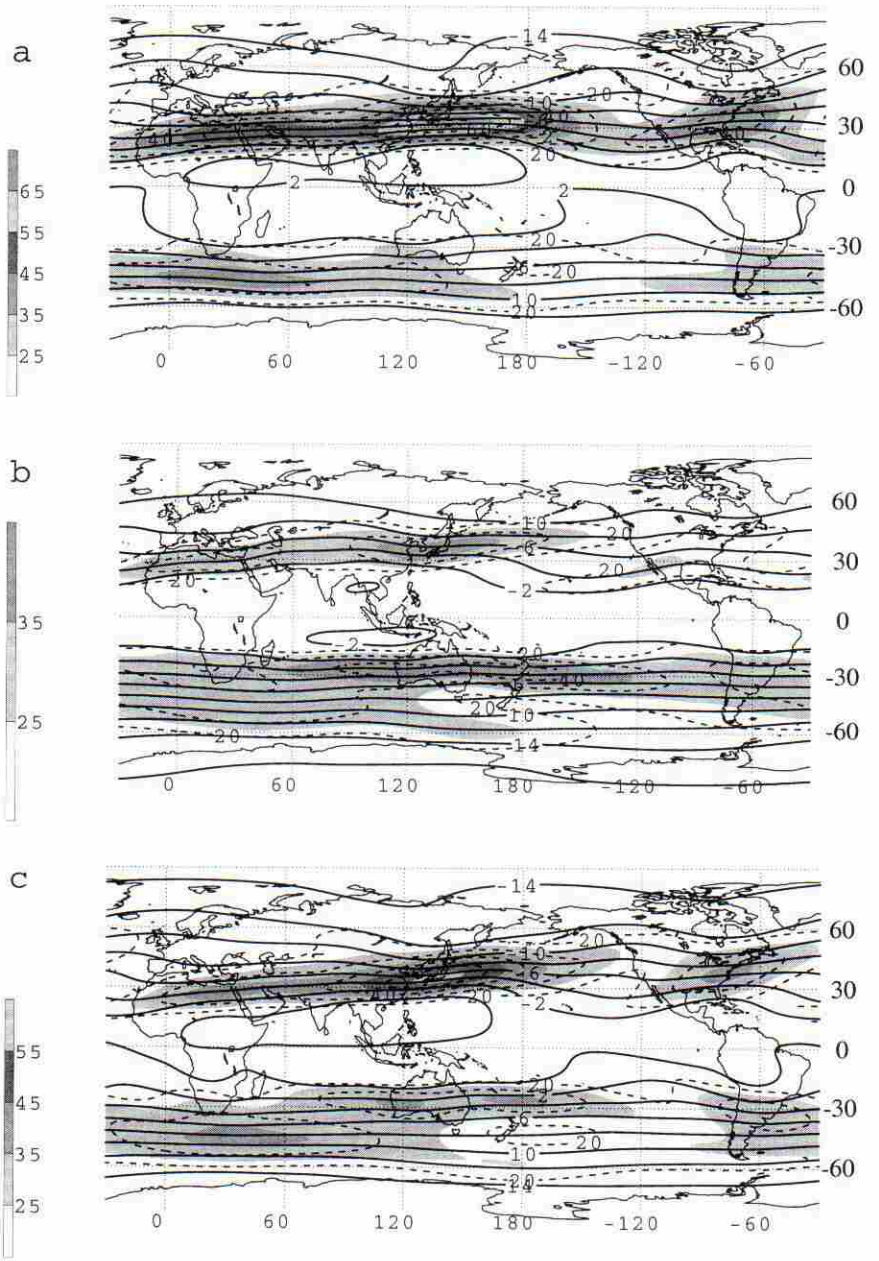

FIG. 6. As in Fig. 1 but for (a) JFM, (b) AMJ, and (c) OND.

variables, and by trying different calculations. However, all attempts resulted in an overall degraded SFI. Our original SFI, as defined in section 2, best described the variability of the split flow for all years but 1998 and is a reliable measure of split flow when the STJ is near its usual intensity.

c. *Zonal wind time series*

A time series of the area-averaged zonal wind for the STJ and PFJ at 200 hPa for the SH cool season from 1958 to 2000 is shown in Fig. 9. The STJ (U_{STJ}) is averaged from 70°E to 130°W and from 25° to 35°S, while the PFJ (U_{PFJ}) is averaged from 150°E to 150°W and from 55° to 65°S. The boxes used for the area averaging are presented graphically in Fig. 2a. Table 4 lists the slopes and correlations of the linear fit, means, and standard deviations for the STJ and PFJ for two time periods: from the IGY to the time of writing, 1958–2000; and the period of time with increased SH satellite data and observations, 1979–2000.

The STJ zonal wind speed from 1958 to 2000 had a downward trend line with a slope of -0.13 m s^{-1} yr^{-1}. This trend decreases slightly when the time period be-

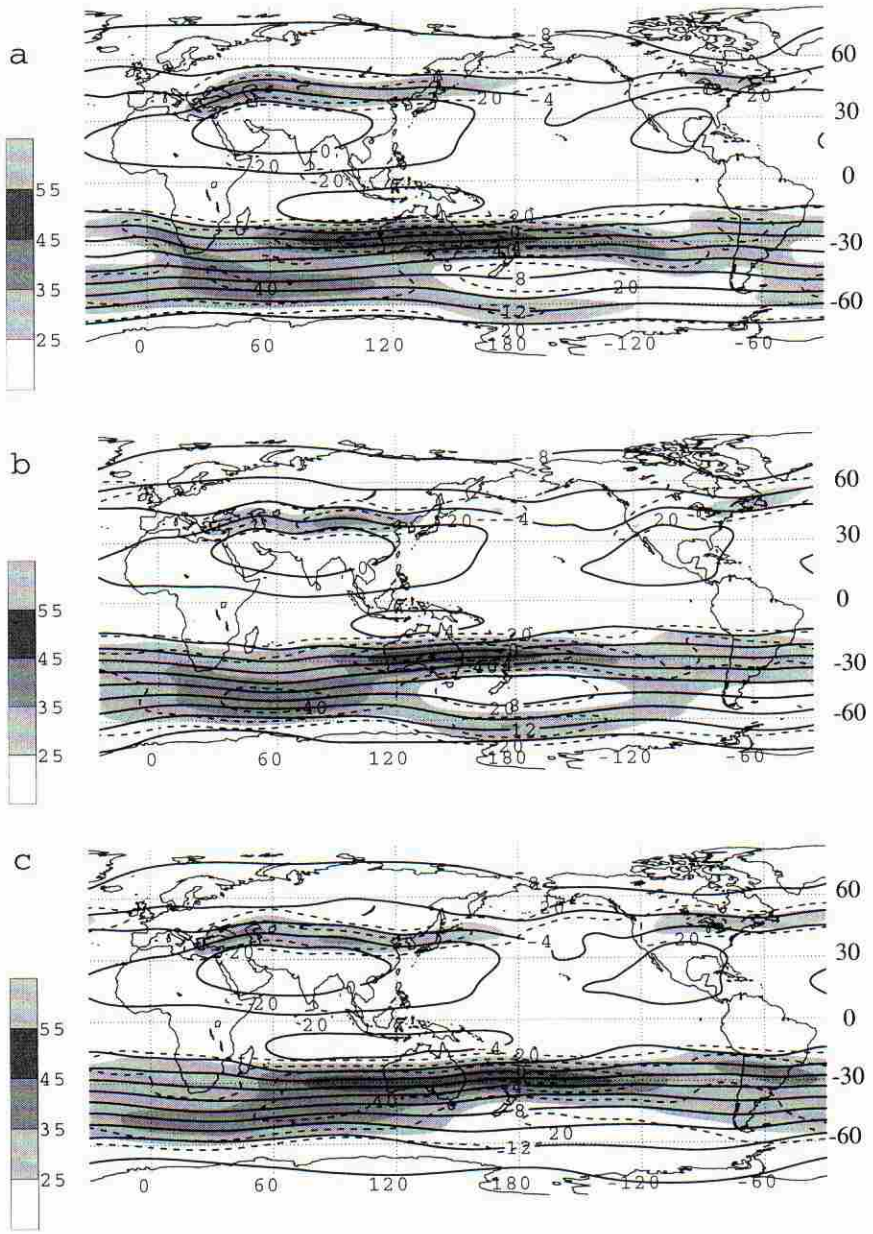

FIG. 7. As in Fig. 1 but for (a) average split flow in 1978 with a 0.2 SFI, (b) strong split flow in 1989 with a −2.0 SFI, and (c) nonsplit flow in 1980 with a 1.5 SFI.

ginning with satellite data is considered, leading to a slope of -0.11 m s^{-1} yr^{-1} (see also Kidson 1999). In contrast to the STJ, the PFJ shows a very slight increasing trend in the magnitude of the zonal wind speed with a trend line slope of 0.02 m s^{-1} yr^{-1} for 1958–2000 and increases to 0.03 m s^{-1} yr^{-1} for 1979–2000. In the time-mean sense, the reanalysis since the IGY does a decent job in detecting and measuring the PFJ. This reaffirms our decision to use the 1958–2000 time period for our study. However, note that the standard deviation of the PFJ increases in magnitude with more recent time periods in comparison with the standard deviation of the STJ. This is especially significant when considering that the average zonal wind speed associated with the PFJ is approximately one-half that of the STJ, indicating a much larger fractional change in the PFJ. The decreased variability suggests that earlier years may not represent the variability of split-flow events as well as later years (see also Hines et al. 1999).

d. Vertical cross sections

A vertical cross section of the zonal wind speed and potential temperature for the JAS climatology is shown

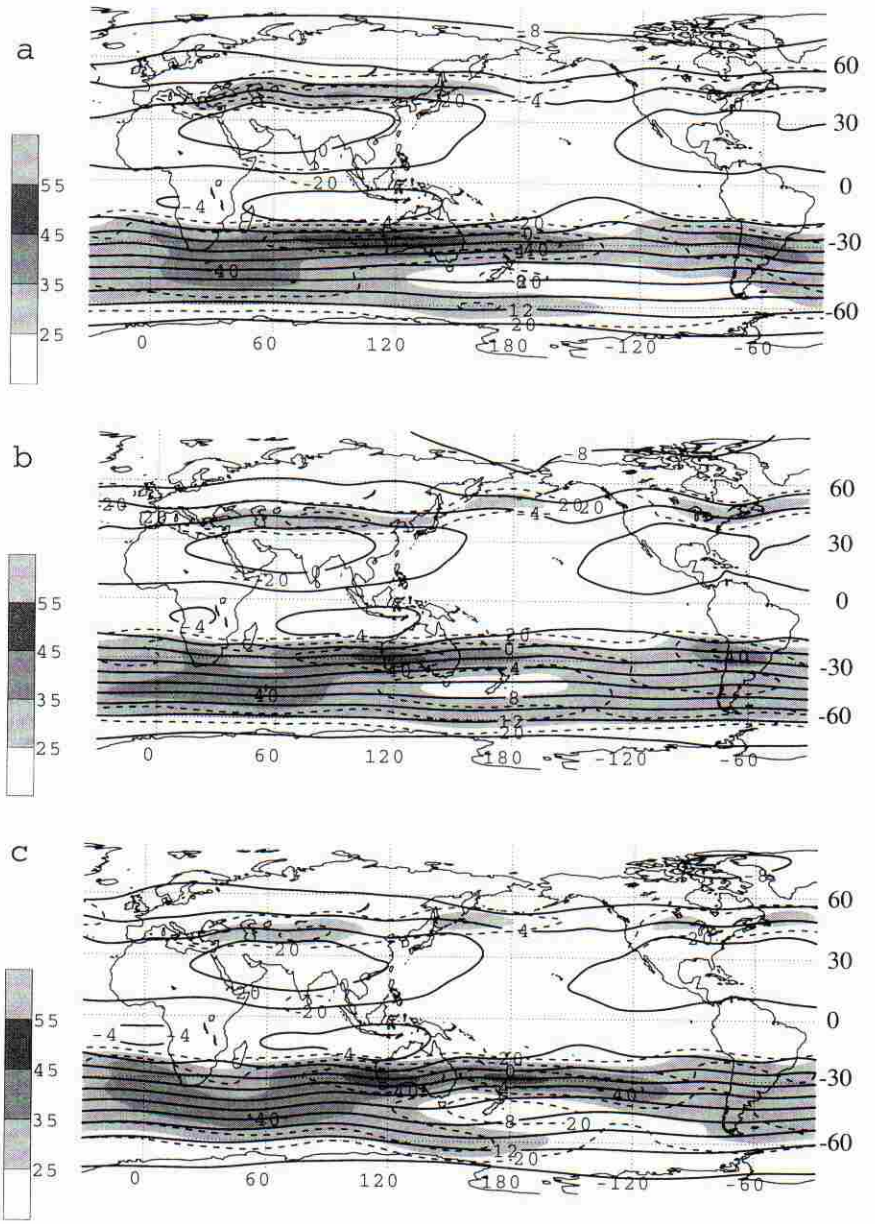

FIG. 8. As in Fig. 1 but for (a) 1975 with a 0.9 SFI, (b) 1998 with a 1.1 SFI, and (c) 1999 with a 1.0 SFI.

in Fig. 10c. The cross section from 87.5°S to 10°N at the date line reveals the climatological mean split jet with a distinct PFJ and STJ in agreement with previous studies (e.g., Taljaard 1972; van Loon 1972a,b,c; Hurrell et al. 1998). The PFJ is located near 65°S and is weakly defined in the mid- and upper troposphere (i.e., 500–200 hPa) with wind speeds increasing from about 20 m s^{-1} at 500 hPa to almost 30 m s^{-1} just above the 200-hPa level. Above this level, the zonal wind speed increases rapidly to a maximum over 80 m s^{-1} near 10 hPa (not shown). The maximum wind speed at the 10-hPa level, as well as the rapid increase in velocity above 200 hPa, indicates that in the climatological mean, the tropospheric portion of the PFJ lies underneath the stratospheric polar night jet surrounding the Antarctic polar vortex. The structure of the PFJ is consistent with the location of the meridional temperature gradient as indicated by the isentropes between 850 and 200 hPa. The strong meridional temperature gradient at 65°S in the troposphere is located in the lowest 300 hPa just equatorward of the polar ice cap, reflecting the strong continental–ocean contrasts (see also Bromwich and Parish 1998).

In contrast to the PFJ, the compact STJ is confined to the 500–100-hPa layer with a maximum in the zonal wind speed over 50 m s^{-1} located at 30°S near 200 hPa.

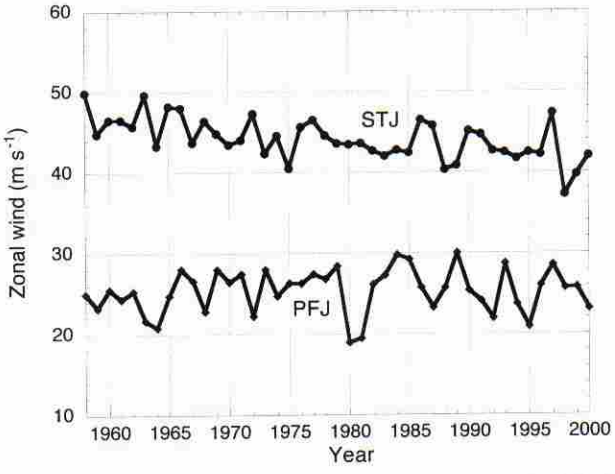

FIG. 9. Times series (1958–2000) of the area-averaged STJ (circles) and PFJ (diamonds) zonal wind (m s^{-1}) at 200 hPa for JAS. The linear fit slopes and correlations are listed in Table 4.

The relatively rapid increase in the zonal wind speed from the 500- to the 200-hPa layer is associated with steeply sloped isentropes (i.e., a strong meridional temperature gradient) in the mid- and upper troposphere (750–300 hPa). The location of the temperature gradient above 750 hPa suggests that the gradient may only be weakly tied to the Australian continent, and that other mechanisms for its maintenance must be considered. The zonal wind speed in the STJ decreases rapidly above the 200-hPa level, consistent with a strong reversal in the direction of the meridional temperature gradient above this level. The meridional temperature gradient reversal indicates that the level of the tropopause rises rapidly equatorward of 30°S in the climatological mean.

In an attempt to further check the validity of the SFI as a quantification of the flow regime on daily timescales as well as seasonal timescales, composites of non-split-flow and split-flow regimes were created. Each day at 0000 UTC from 1958 to 1999 (excluding PAOBS years) where the normalized SFI was greater than 1.5 was used to create the non-split-flow composite ($n = 201$) and each day where the normalized SFI was less than -1.5 was used to create the split-flow composite ($n = 134$).

A vertical cross-section composite of the days characterized by nonsplit flow is shown in Fig. 10a. The wind maximum associated with the STJ is located at 35°S with no indication of a significant PFJ in the troposphere. While there is a strong wind maximum near 60°S at 50 hPa, this wind maximum is a response to stratospheric dynamics and is not connected to any significant tropospheric temperature gradient. All the significant baroclinicity for the non-split-flow regime is located in the mid- and upper troposphere near 35°S. The structure of the STJ is largely unchanged, although its location is displaced poleward relative to climatology and to the split-flow composite.

A vertical cross section of the zonal wind and potential temperature for the composite split-flow regime is given in Fig. 10b. Two distinct wind maxima are located at 27.5° and 62.5°S. The PFJ and STJ are located in approximately the same position as climatology (Fig. 10c). However, the PFJ in the split-flow regime is stronger than climatology with the 20 m s^{-1} isotach extending down to 850 hPa in the split-flow composite but to only 500 hPa in the climatology. This increase in the PFJ strength is consistent with the more steeply sloped isentropes in the split-flow composite. Significantly, there is very little difference in the structure and location of the split-flow STJ from climatology. This supports our earlier assertion that the STJ is a quasi-steady feature of the SH cool season and that the characterization of the split-flow regime is largely dependent on the presence/absence and strength of the PFJ.

In order to depict the temperature and zonal wind differences among these cross sections, Fig. 11 contains the composite nonsplit flow minus JAS climatology (Fig. 11a), composite split flow minus JAS climatology (Fig. 11b), and composite nonsplit flow minus composite split flow (Fig. 11c). In Fig. 11a the poleward shift of the STJ is denoted by a positive wind anomaly from 30° to 45°S. The anomaly is a maximum between 200 and 250 hPa. With no PFJ in the non-split-flow composite, the location of the climatological PFJ is outlined by a negative wind anomaly from 55° to 70°S. This anomaly is a maximum between about 350 and 200 hPa. The temperature anomalies show a slight warming equatorward of the STJ below 200 hPa and a cooling above this level. A slight cooling exists below 300 hPa poleward of the STJ to the center of the climatological PFJ, with warming above 250 hPa. A strong warm anomaly centered at 75°S exists poleward of the PFJ anomaly and extends from 350 hPa to the surface, reflecting the destruction of the meridional temperature gradient associated with the PFJ. These temperature anomalies near the date line are consistent with cold air being displaced off the Antarctic coast as the flow pattern amplifies poleward of Australia. The evolution of these cold surges poleward of New Zealand will be

TABLE 4. Statistics on the STJ and PFJ.

	Slope (m s^{-1} yr^{-1})		Correlation coefficient of the linear fit		Mean (m s^{-1})		Std dev (m s^{-1})	
	STJ	PFJ	STJ	PFJ	STJ	PFJ	STJ	PFJ
1958–2000	−0.13	0.02	0.68	0.37	44.1	25.3	2.7	2.7
1979–2000	−0.11	0.03	0.28	0.06	42.8	25.4	2.3	3.2

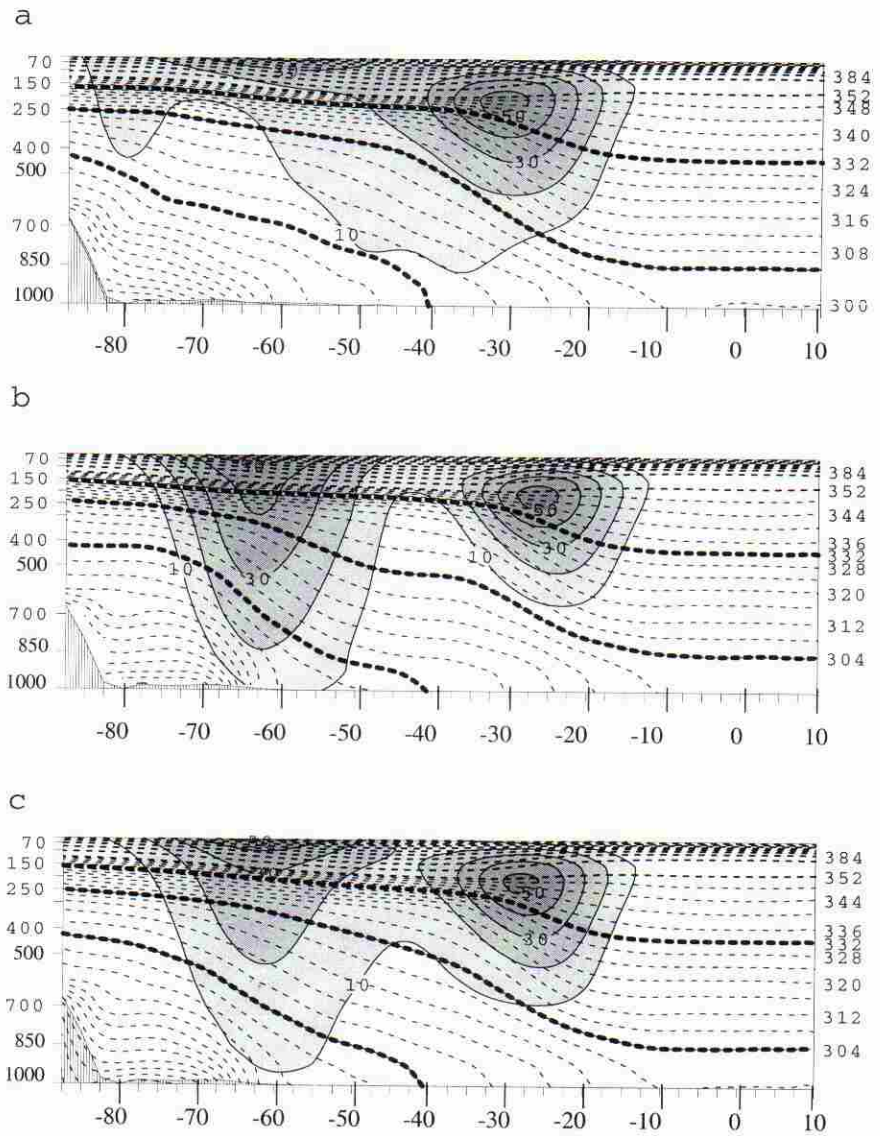

FIG. 10. Vertical cross section of the zonal wind isotachs and potential temperature from 1000 to 10 hPa taken at the date line between 87.5°S and 10°N for (a) composite nonsplit flow (201 members), (b) composite split flow (134 members), and (c) JAS climatology. Isotachs (solid) are contoured and shaded every 10 m s^{-1} above 10 m s^{-1}. Isotherms (dashed) are contoured every 4 K for values less than 352 K and every 16 K above 352 K, with the 284, 304, and 332 K isotherms plotted in a thicker line. Reanalysis terrain representation is hatched; note that since no terrain representation was available for the climatology in (c), the graphics software allows the isotherms to incorrectly intersect with the terrain plotted from the composites.

documented in an upcoming paper addressing the synoptic modulation of the split-flow regimes. The composite split flow minus JAS climatology in Fig. 11b is the mirror image of Fig. 11a. The poleward side of the STJ has a negative zonal wind anomaly and the PFJ has a positive zonal wind anomaly. Little temperature difference is apparent equatorward of the STJ. Between the STJ and PFJ latitudes, a warm anomaly stretches below 250 hPa and a cold anomaly lies above 250 hPa, consistent with the presence of a blocking anticyclone in this region. Poleward of the PFJ zonal wind anomaly a cold anomaly sits below 300 hPa, maximized at the base of the PFJ between 950 and 700 hPa, suggestive of relatively cold air trapped near the edge of the Antarctic ice sheet.

In Fig. 11c, the difference between the non-split-flow and split-flow composites is a pronounced enhancement of the pattern noted in Fig. 11a, the nonsplit flow minus climatology. The poleward shift of the STJ in nonsplit flow is seen in the 10 m s^{-1} negative zonal wind anomaly equatorward of 30°S centered at 200 hPa and a 25 m s^{-1} positive anomaly centered at 37.5°S. The PFJ char-

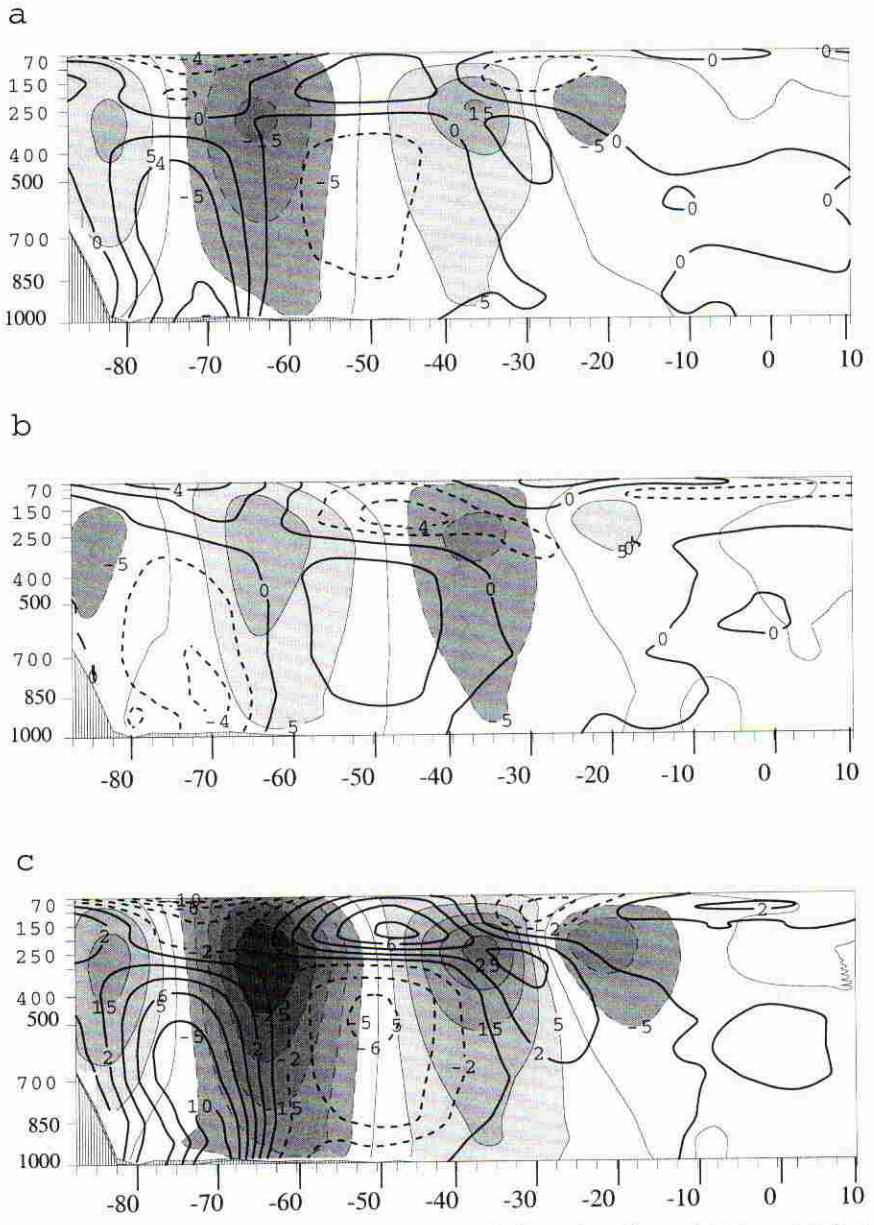

FIG. 11. Vertical cross section of anomalous zonal wind isotachs and potential temperature from 1000 to 10 hPa taken at the date line between 87.5°S and 10°N for (a) composite nonsplit flow minus JAS climatology, (b) composite split flow minus JAS climatology, and (c) composite nonsplit flow minus composite split flow. Zonal wind speed shaded every 5 m s^{-1} above 5 m s^{-1} with light (dark) shading for positive (negative), or westerly (easterly) anomalies. Isotherms are solid (dashed) every 2°C for positive (negative) anomalies.

acteristic of split flow appears in the deep 25 m s^{-1} negative anomaly at 65°S from 150 to 450 hPa, while the 15 m s^{-1} anomaly penetrates to nearly 850 hPa. The temperature anomalies below 250 hPa reveal a weak warm anomaly equatorward of the STJ, a strong cold anomaly between the STJ and PFJ, and a strong warm anomaly poleward of the PFJ anomaly core. As compared with split flow, nonsplit flow is characterized by warmer temperatures at higher latitudes, while cooler air is located from 40° to 60°S. Above 250 hPa the anomalies reverse, with cold anomalies above the high-latitude warm anomaly, and a warm anomaly above the midlatitude cold anomaly.

The vertical structure of the jets revealed in the climatologies, composites, and anomalies lends credence to the selection of 200 hPa for calculation of the SFI. The composites and climatology in Fig. 10 show that the maximum zonal velocity associated with the STJ is

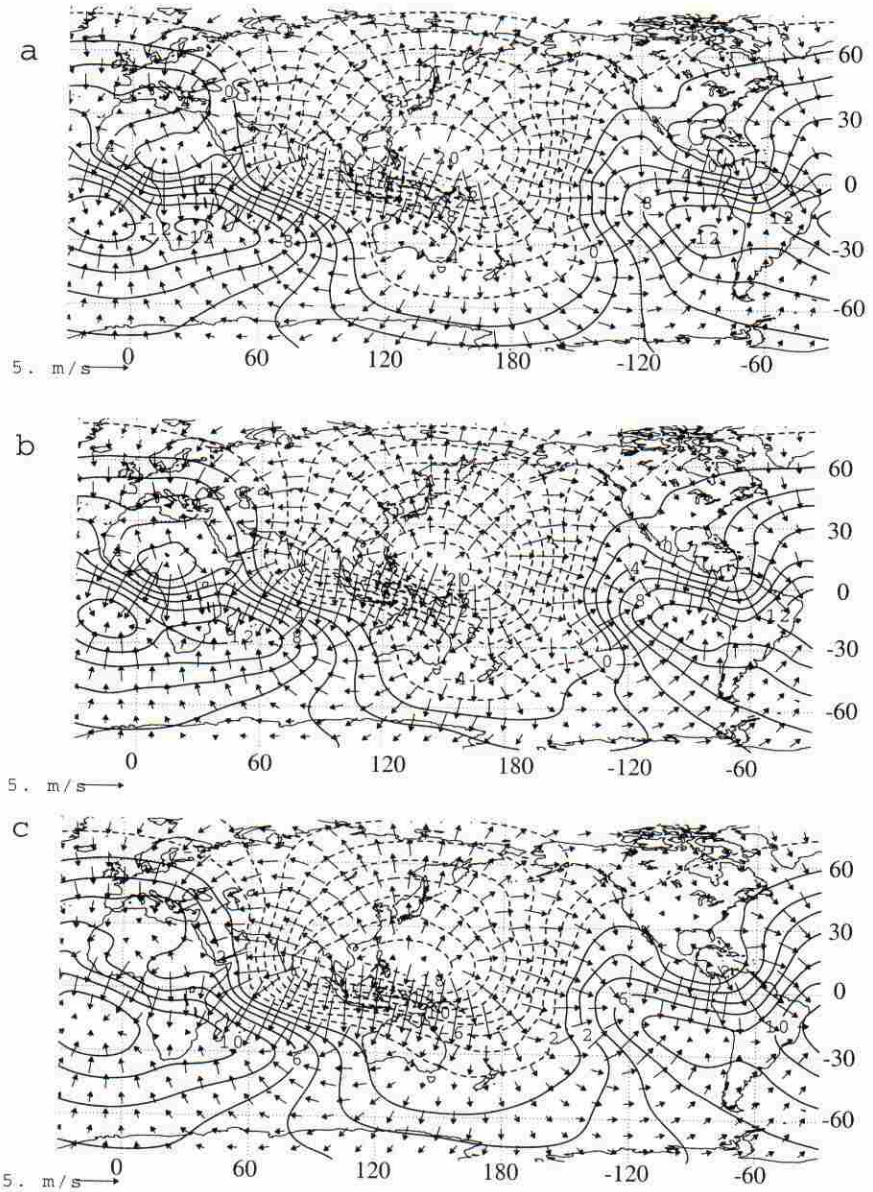

FIG. 12. The 200-hPa velocity potential and vectors of the divergent wind for (a) composite nonsplit flow (201 members), (b) composite split flow (134 members), and (c) JAS climatology. Velocity potential contoured every 2×10^6 m^2 s^{-1}.

located near 200 hPa. Furthermore, the 200-hPa level is below the location where the zonal wind associated with the stratospheric polar night jet starts to rapidly increase upward. This ensures that we are basing our SFI calculations on the tropospheric reflection of the PFJ and not the stratospheric polar night jet. Given the apparent lack of connection of the stratospheric jet to any tropospheric temperature gradient, we feel it is unlikely that the presence or location of the stratospheric polar night jet plays a significant role in the modulation of synoptic-scale disturbances controlling the sensible weather.

e. Velocity potential and streamfunction

The strength and location of the STJ and the associated meridional temperature gradient can in part be understood by an examination of the 200-hPa global velocity potential and divergent wind (Fig. 12c). Figure 12c shows strongly divergent outflow from the anticyclone centered over the western Pacific warm pool. The time-mean cross-equatorial flow associated with the divergence approaches 8 m s^{-1} over Indonesia. The location of the 200-hPa STJ wind maximum just south of the divergent outflow (Fig. 13c) strongly suggests that

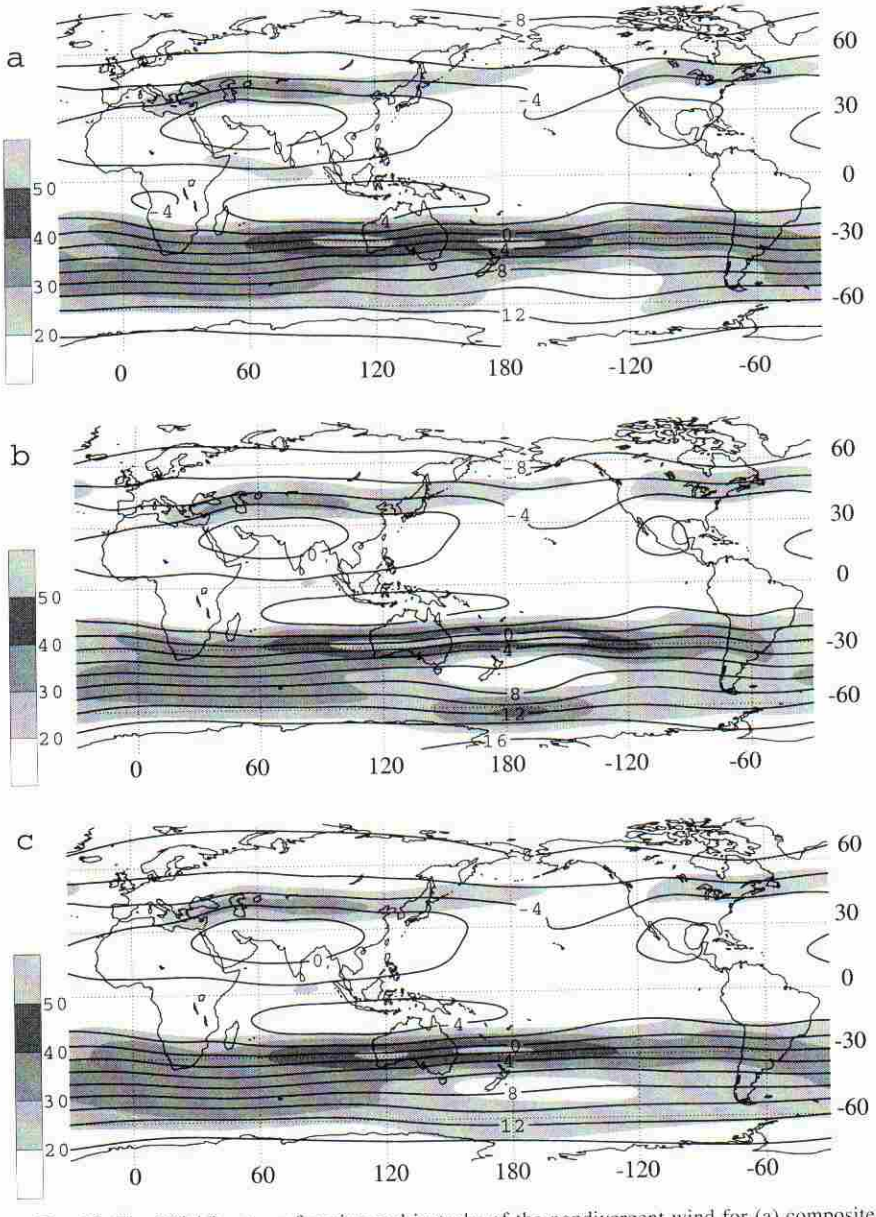

FIG. 13. The 200-hPa streamfunction and isotachs of the nondivergent wind for (a) composite nonsplit flow (201 members), (b) composite split flow (134 members), and (c) JAS climatology. Streamfunction is contoured every 2×10^7 m^2 s^{-1}, and isotachs are shaded every 10 m s^{-1} above 20 m s^{-1}.

the STJ is partly maintained by Coriolis-torqued outflow from the 200-hPa anticyclone situated over the western Pacific warm pool, concurring with results presented by Newton (1972) and Hurrell et al. (1998). This interpretation is further supported by the high correlation between the cross-equatorial flow (V_{EQU}) and the strength of the zonal wind in the STJ (U_{STJ}) as shown in Table 2. At 850 hPa (not shown), strong convergent inflow is located over the western Pacific warm pool and below the 200-hPa divergent outflow. The STJ is essentially nonexistent at 850 hPa (Fig. 14c), indicating that the baroclinicity at this latitude is confined to the mid- and upper troposphere as shown in Fig. 10c. In contrast, a high-latitude wind maximum of over 12 m s^{-1} at 850 hPa poleward of New Zealand suggests that lower-tropospheric dynamics are important in the PFJ, in spite of the fact that the maximum in the zonal wind is located upward of 10 hPa.

In the composite of the velocity potential for nonsplit flow (Fig. 12a) and split flow (Fig. 12b) the location of the center of divergent outflow remains basically unchanged from climatology. Both the nonsplit flow and split flow have strong cross-equatorial outflow equatorward of the STJ. The velocity potential

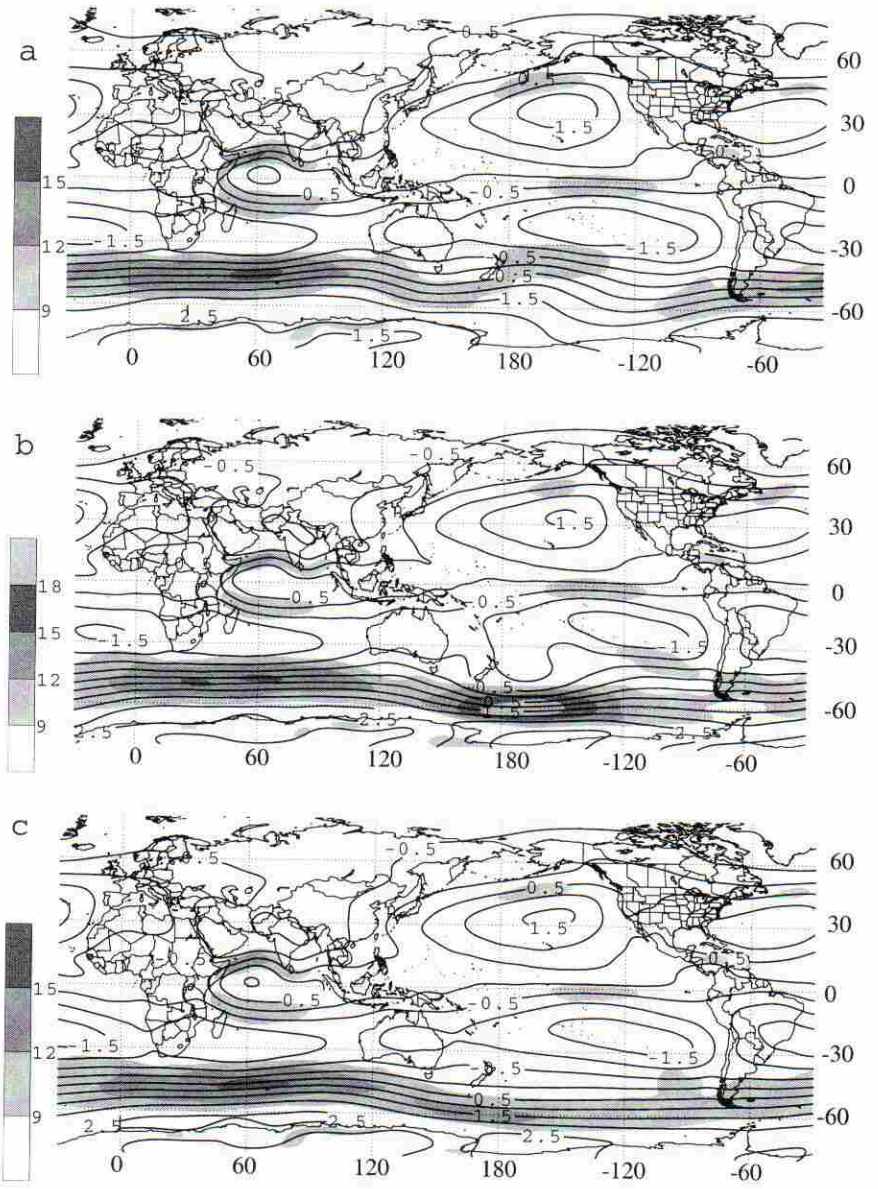

FIG. 14. As in Fig. 13 but for 850 hPa contoured every 0.5 × 10^7 m^2 s^{-1} and shaded every 3 m s^{-1} above 9 m s^{-1}.

gradient and associated outflow poleward of the southern tip of New Zealand are slightly stronger in the split-flow composite than in either the nonsplit flow or climatology. The stronger outflow is located equatorward of the composite split-flow PFJ wind maximum (Fig. 13b) and is consistent with the presence of a stronger PFJ. As noted at the date line in Fig. 10a, no PFJ can be found in the South Pacific 200-hPa streamfunction non-split-flow composite (Fig. 13a). Instead, the climatological gradient associated with the PFJ in a split-flow regime has been replaced by a negatively tilted trough at higher latitudes. Note that the southwesterly flow poleward of New Zealand is suggestive of cold surges in this region. This evolution of cold surges into the region will be illustrated in a forthcoming companion paper. The non-split-flow STJ (Fig. 13a) has two separate 50 m s^{-1} cores, one off the western coast of Australia and one equatorward of New Zealand, coincident with troughs at higher latitudes, both centered at 30°S. A high-latitude ridge from New Zealand to 170°W in the split-flow composite (Fig. 13b) strengthens the streamfunction gradient associated with the PFJ. The split-flow STJ has a strong core (50 m s^{-1}) stretching from near 100°E to 140°W at 25°S. Unlike the findings of Chen et al. (1996), our composite shows a strong

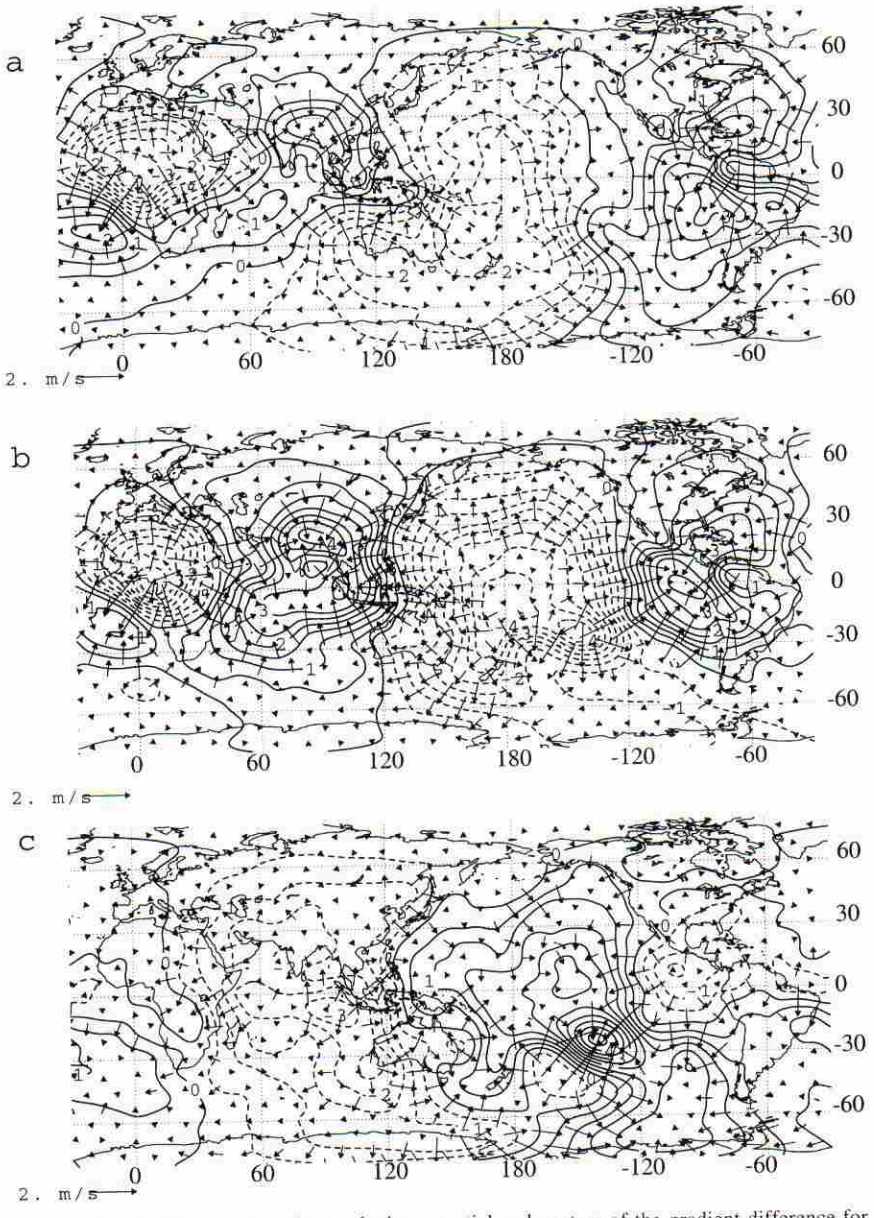

FIG. 15. The 200-hPa anomalous velocity potential and vectors of the gradient difference for (a) composite nonsplit flow minus JAS climatology, (b) composite split flow minus JAS climatology, and (c) composite nonsplit flow minus composite split flow. Velocity potential contoured every 0.5×10^6 m^2 s^{-1}.

STJ paired with a strong PFJ. Their result of a weaker STJ associated with a strong PFJ may be the product of a shorter time series.

At 850 hPa the high-latitude wind maximum exceeds 18 m s^{-1} in the split-flow composite (Fig. 14b). Strong northwesterly flow poleward of Australia to the date line and northerly flow across New Zealand imply warm air advection in the South Pacific toward the high-latitude jet maximum. Southwesterly flow exits the equatorward side of the low-level jet core toward 120°W. In the nonsplit-flow composite (Fig. 14a), the high-latitude flow is southwesterly between the longitudes of Australia and New Zealand, suggesting warm air intrusions into the polar regions, with a 9 m s^{-1} wind maximum occurring at 35°S east of New Zealand, implying a shift equatorward in the low-level baroclinicity.

The anomaly fields for the velocity potential appear in Fig. 15. In the non-split-flow-minus-climatology anomaly (Fig. 15a), a negative anomaly is located east of Australia and equatorward of New Zealand. This region stretches across the equator toward 30°N, southward toward 60°S, and hooks westward around the south side of Australia. This pattern indicates slightly stronger outflow than climatology across this region during non-

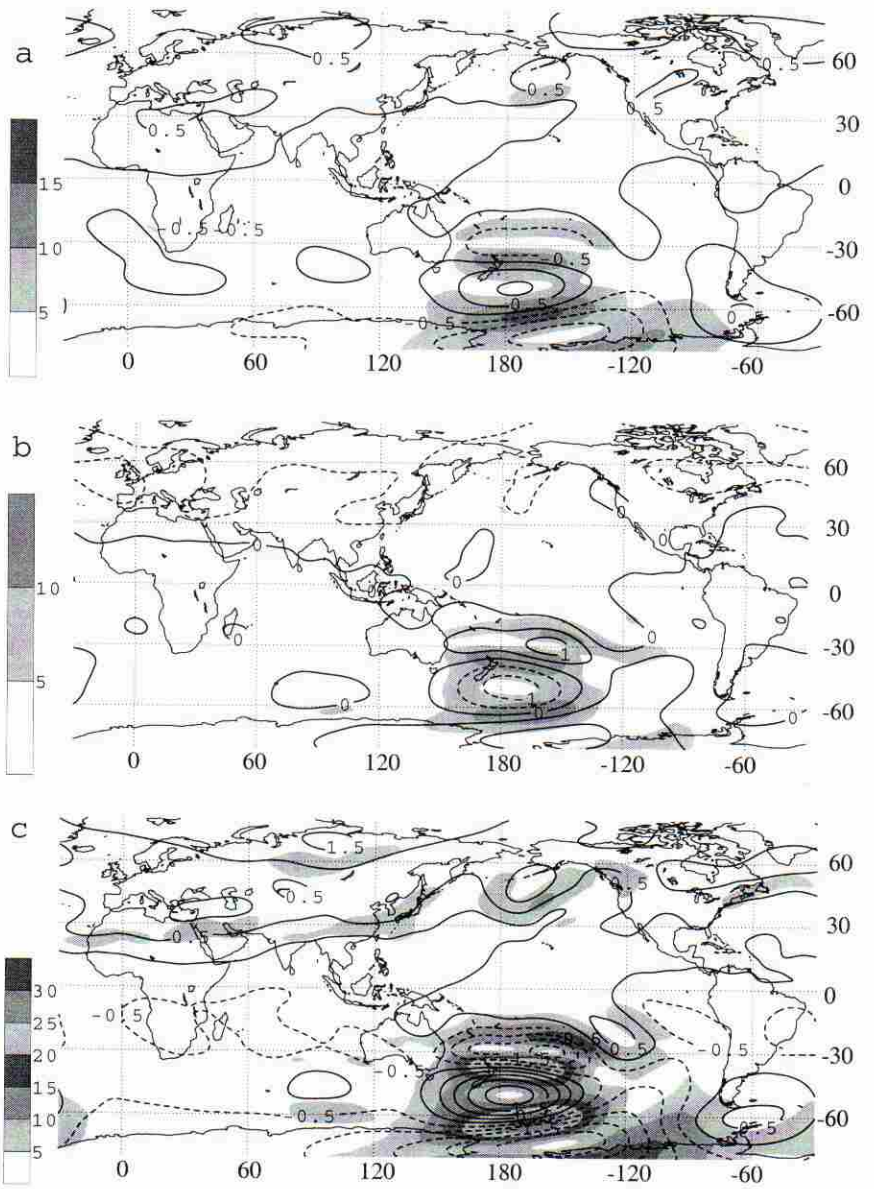

FIG. 16. The 200-hPa anomalous streamfunction and isotachs of the gradient difference for (a) composite nonsplit flow minus JAS climatology, (b) composite split flow minus JAS climatology, and (c) composite nonsplit flow minus composite split flow. Streamfunction is contoured every 0.5×10^7 m^2 s^{-1}, and the gradient of the difference field is shaded every 5 m s^{-1} above 5 m s^{-1}.

split-flow events. The split-flow anomaly has a negative anomaly centered over the date line across the South Pacific, but does not extend as far south as the non-split-flow anomaly.

The streamfunction anomaly fields at 200 hPa (Fig. 16) and 850 hPa (Fig. 17) highlight the sharp contrasts between the non-split-flow and split-flow regimes with bull's-eyes on the SH South Pacific. In the non-split-flow anomaly (Fig. 16a), a positive streamfunction anomaly (clockwise flow) poleward of New Zealand at the date line reflects the relatively weak PFJ, with 15 m s^{-1} anomalous easterly flow located near the climatological position of the PFJ. A slight strengthening of the STJ (10 m s^{-1}) on its poleward side and a weakening (easterly anomaly) on the STJ equatorward side indicates a poleward shift in the location of the STJ. The positive stream function anomaly extends down through the troposphere to 850 hPa (Fig. 17a). The 200-hPa split-flow anomaly (Fig. 16b) has anomalies of nearly the same magnitude but in the opposite sense (counterclockwise flow) as the nonsplit flow. A 10 m s^{-1} westerly anomaly at 60°S is located near the climato-

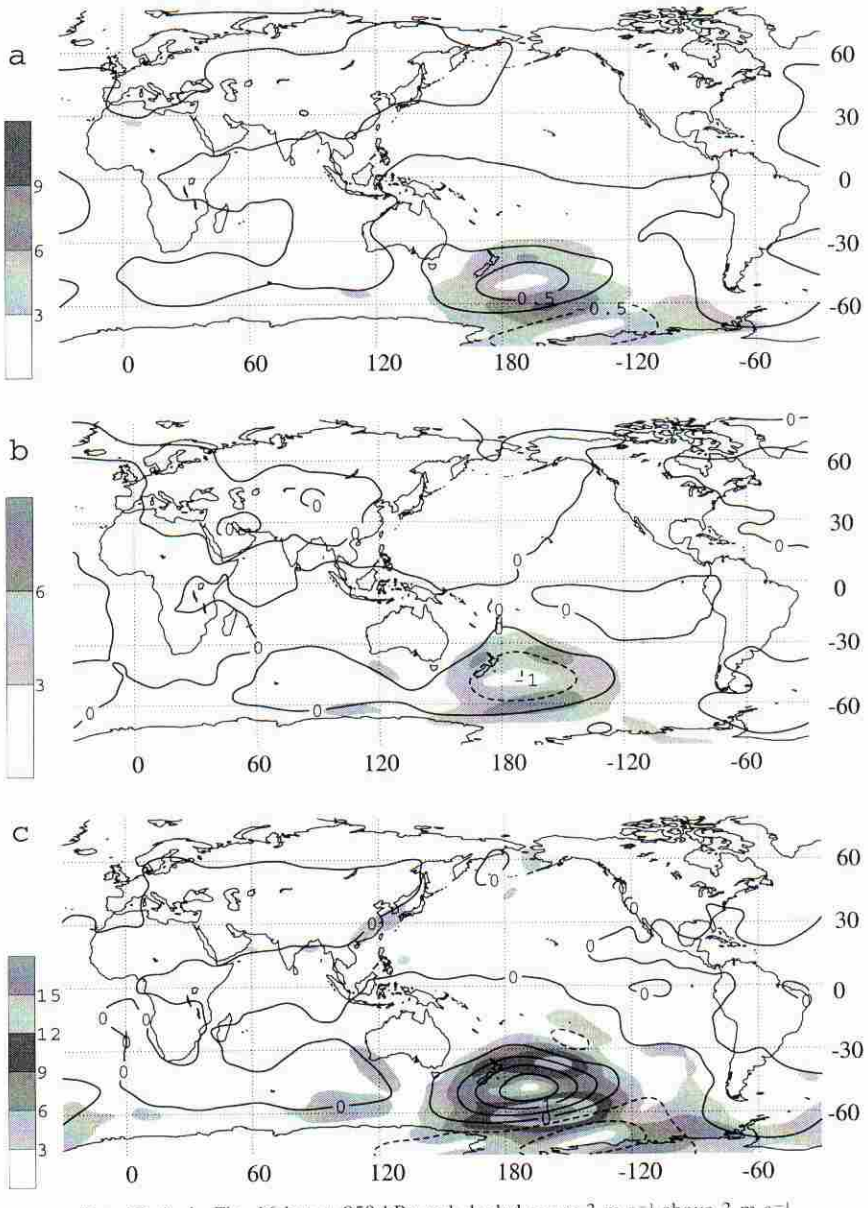

FIG. 17. As in Fig. 16 but at 850 hPa and shaded every 3 m s^{-1} above 3 m s^{-1}.

logical position of the PFJ. A 10 m s^{-1} easterly anomaly at 35°S occurs at the gap and is suggestive of a blocking high in this region. The easterly anomaly and a 10 m s^{-1} westerly anomaly at 25°S indicate an equatorward shift of the STJ. At 850 hPa (Fig. 17b) the negative anomaly persists, outlining the depth of the PFJ. The non-split-flow-minus-split-flow anomaly in Figs. 16c and 17c accentuates the flow differences between these regimes. On the equatorward side of the positive anomaly the westerly flow anomaly exceeds 25 m s^{-1} in association with the poleward-shifted STJ, while on the poleward side of the positive anomaly, the easterly flow anomaly reaches upward of 30 m s^{-1} reflecting the complete destruction of the PFJ in non-split-flow regimes. On either side of the positive anomaly equally strong negative anomalies contribute to the strength of the anomalous flow, to the shift of the STJ, and to the dissipation of the PFJ. Figure 17c is an amplification of the non-split-flow-minus-climatology anomaly of Fig. 17a.

5. Discussion

To help put our results in perspective we now compare and contrast the atmospheric thermal structure and 1000-hPa height field in the SH. Figure 18c displays the JAS climatological 1000–400-hPa thickness and 1000-hPa heights for the SH. Although the 1000–400-hPa thickness pattern is fairly zonal, regions of enhanced baroclinicity exist over southern South America, pole-

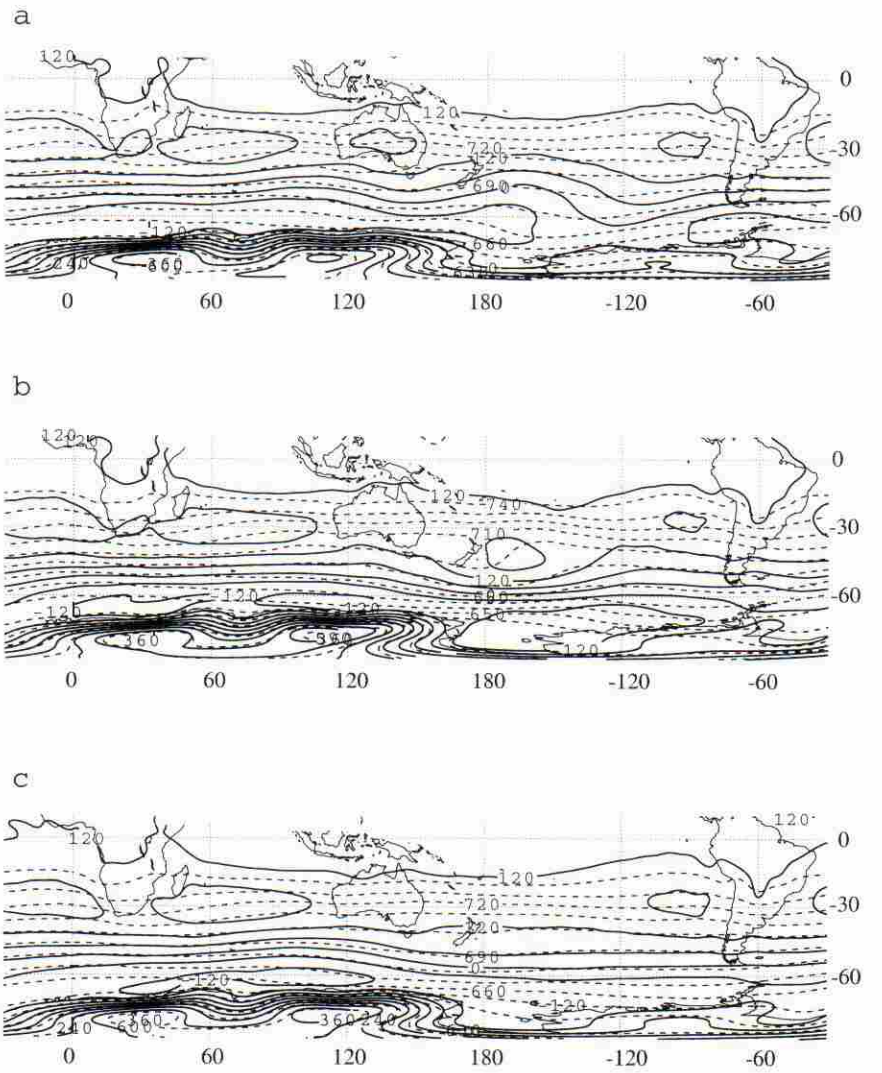

FIG. 18. The SH 1000-hPa heights and 1000–400-hPa thickness for (a) composite nonsplit flow (201 members), (b) composite split flow (134 members), and (c) JAS climatology. Heights (solid) are contoured every 60 gpm, and thickness (dashed) is contoured every 10 dam.

ward of South Africa, and across central sections of Australia. The lower latitudes of South Africa and South America serve as warm perturbations of the mean zonal thickness gradient near 30°S, thereby enhancing the baroclinicity poleward of these landmasses. Australia, on the other hand, represents a relative cold anomaly with respect to the southwest Pacific warm pool to its north. This configuration allows the continents to serve as "land anchors" (Taljaard 1972; H. van Loon 2000, personal communication) for the STJ. Other features of note include a region of northwesterly flow and weak warm air advection poleward of Australia and New Zealand, just south of a region of difluence in the thickness field. The resulting baroclinicity at high latitudes in conjunction with the strong thickness gradient equatorward of New Zealand represents the time-mean signature of a split-flow regime between the longitudes of Australia and South America. The implied weak upper-tropospheric flow located near and over New Zealand is an area that has been shown to be favored for episodes of strong blocking (e.g., Trenberth and Mo 1985; Mo et al. 1987; Trenberth 1986a, 1991). In the 1000-hPa height field, oceanic highs stretch across the south Indian and South Atlantic Oceans, with another high situated off the western coast of South America.

In contrast to the climatological mean, the nonsplit composite (Fig. 18a) indicates a trough in the thickness field near the date line accompanied by southwesterly flow at high and midlatitudes. The broad subtropical ridging present in the 1000-hPa height field in the climatological mean (Fig. 18c) has been suppressed equatorward, with a closed anticyclone now located over Australia. Concurrently, the flow both upstream and downstream of the date line shows considerable merid-

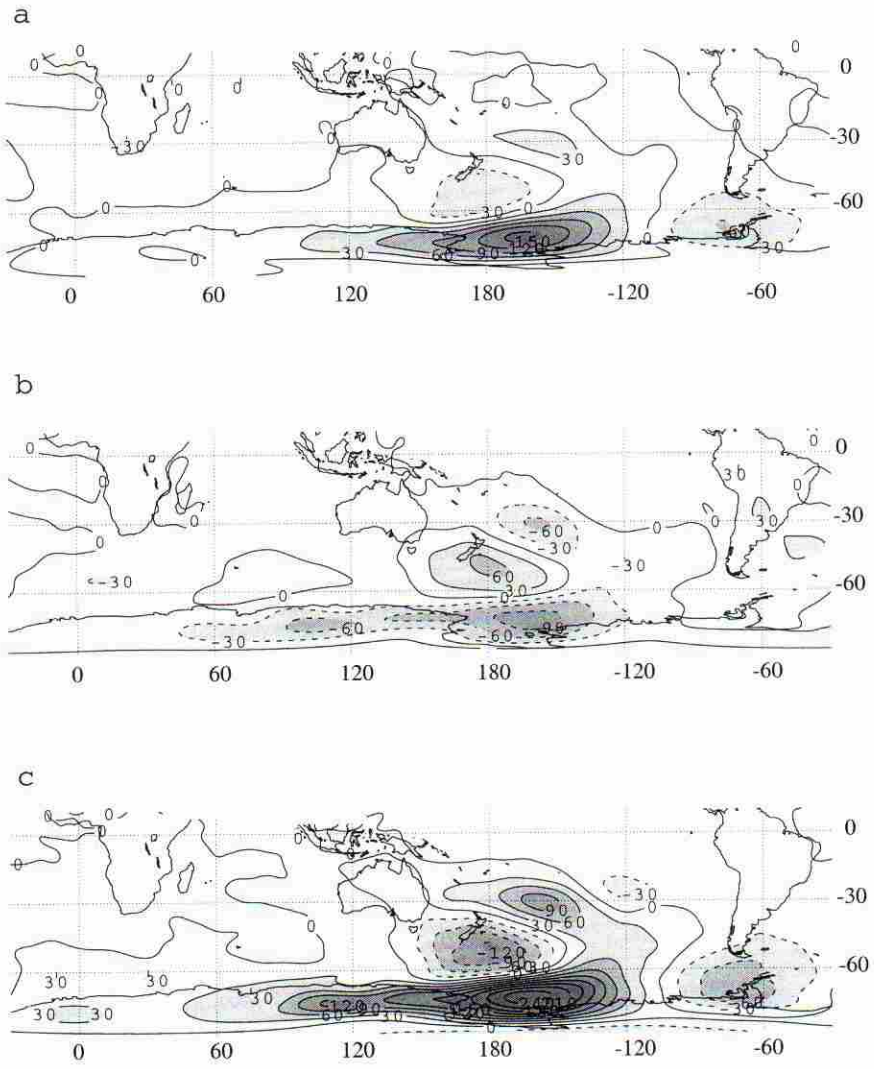

FIG. 19. The SH anomalous 1000–400-hPa thickness for (a) composite nonsplit flow minus JAS climatology, (b) composite split flow minus JAS climatology, and (c) composite nonsplit flow minus composite split flow. Thickness anomalies are contoured every 30 gpm and shaded for values greater than ±30 gpm.

ional amplification versus the climatological mean. The 690-dam thickness contour has shifted several degrees equatorward near and just to the east of New Zealand. At the same time, the 660-dam thickness has shifted farther poleward near 180°W. The resulting difluence in the thickness field represents the destruction (displacement) of the PFJ in this region, and the northwesterly flow and colder thicknesses are suggestive of cold air being displaced equatorward from Antarctica.

Figure 18b shows the composite for enhanced split flow. A closed anticyclone in the 1000-hPa height field lies east of New Zealand, suggestive of the enhanced blocking activity associated with strongly split flow. The 700-dam thickness contour has been displaced poleward of New Zealand, while the 640-dam thickness contour is displaced equatorward off the Antarctic coastline near 180°W. As a result, the thickness gradient at high latitudes between 120°W and 120°E is strengthened considerably with respect to climatology and in contrast to the non-split-flow composite. This enhanced thickness gradient is consistent with a stronger PFJ and occurs as a result of broad warm air advection ahead of a positively tilted trough in the south Indian Ocean. By far, the most significant differences in the height and thickness fields occur poleward of 30°S, indicating once again that differences in the PFJ are the most defining factors in quantifying the presence or absence of split flow in the South Pacific.

The 1000–400-hPa thickness anomaly fields for the split-flow and non-split-flow composites are given in Figs. 19a and 19b, respectively. Most of the significant thickness anomalies at midlatitudes seem to be confined between 120°W and 120°E, and are largely associated with the dissipation (strengthening) of the PFJ in Fig. 19a (Fig.

19b) and the displacement of the STJ poleward (equatorward). The warm thickness anomaly of 150 m near 165°W in conjunction with the cold anomaly of 30 m just poleward of New Zealand represents a relaxing of the temperature gradient of approximately 6×10^{-6} °C m^{-1} [6°C (1000 km)$^{-1}$] (note that a 60-m change in thickness is equivalent to a 2.2°C change in the mean temperature for the 1000–400-hPa layer). Using thermal wind arguments, this relaxation of the temperature gradient corresponds to a decrease of approximately 15 m s^{-1} in the wind shear of this layer and accounts for the weakening of the PFJ in this region. Differences in the strength and position of the STJ are less pronounced, although the temperature gradient associated with the STJ has been displaced poleward near 170°W.

In Fig. 19b (split flow), the pattern of the thickness anomalies has been reversed, in agreement with the anomalous potential temperature signatures given in Fig. 11. In the split-flow composite, the cold anomaly at 75°S and 160°W, in conjunction with the warm thickness anomaly east of New Zealand, represents an increase of the climatological temperature gradient associated with the PFJ of approximately 5°C. This temperature gradient increase corresponds to an increase in the wind shear of approximately 13 m s^{-1} in the 1000–400-hPa layer. The temperature gradient associated with the STJ has been displaced slightly equatorward of 30°S. The warm anomaly near New Zealand is located in the gap region and may be associated with anomalous blocking high activity in the midlatitudes.

Figure 19c represents the differences in the thickness pattern between the two flow regimes. Since the anomaly patterns in Figs. 19a and 19b are similar spatially and opposite in sign, the resulting differences between the two flow regimes are quite dramatic. The thickness anomaly patterns represent a change in the temperature gradient in the higher latitudes of approximately 10×10^{-6} °C m^{-1} [10°C (1000 km)$^{-1}$], which is equivalent in magnitude to the climatological mean temperature gradient. This anomaly is an indication that the SFI is quantifying a clear and significant perturbation, or departure from the climatological mean. This result reinforces our confidence in the performance of the SFI.

6. Conclusions

Although most previous studies of SH flow regimes have emphasized the documentation and understanding of the time-mean flow signatures, relatively little has been done toward examining the structure and synoptic evolution of the predominant SH split jet. We have used the newly available NCEP–NCAR reanalyses to update and expand on previous climatologies of the prevailing cool-season flow regime in the SH and to objectively quantify and evaluate the SH split jet. Our climatology reaffirmed the presence of a split jet that occurs preferentially in the South Pacific to the east of Australia. The separation of a single zonal jet into a PFJ and STJ begins in the south Indian Ocean. The PFJ curves poleward, to the southeast of the west Australian coast, eventually paralleling the Antarctic coast at about 60°S near the date line. Meanwhile, the STJ stretches zonally along 25°–30°S across central Australia and continues eastward, equatorward of New Zealand, to South America. Onset of the split jet begins in the SH fall as the STJ becomes established over the lower latitudes, while dissipation occurs in SH spring as the baroclinic zone in lower latitudes weakens.

Our study has endeavored to create an objective index to quantify the degree to which the flow in the South Pacific is split. Hovmöller plots of both the 200-hPa zonal wind speed and relative vorticity revealed that the STJ is a quasi-steady feature of the SH cool season, while the location and strength of the PFJ tended to be more variable. A minimum in the zonal wind speed and a maximum in the anticyclonic relative vorticity occurred in the gap between the PFJ and the STJ in the South Pacific. An analysis of the Hovmöller plots led to the development of a split-flow index (SFI) consisting of three separate parameters measuring the 200-hPa relative vorticity at different latitude bands in the South Pacific. The resulting SFI value is negative during periods of split flow, as the cyclonic (negative) vorticity is maximized over both the PFJ and the STJ, and the anticyclonic (positive) vorticity is accentuated in the gap between the two jets. However, when the PFJ is weak, the normalized SFI becomes positive as the cyclonic relative vorticity in the southernmost latitude band lessens and the relative vorticity in the gap region becomes cyclonic.

The normalized SFI agreed favorably with a subjective classification of the flow regime, with the one exception of 1998. The exception was due to an anomalously weak STJ, unprecedented in the 43-yr climatology. All attempts to refine the SFI to account for this anomaly resulted in an overall degradation in the performance of the SFI.

The SFI was correlated with teleconnection indices such as the SOI, PDO, and AAO. The SOI is only weakly correlated with the SFI, suggesting that split-flow conditions in the South Pacific are not strongly modulated by El Niño or La Niña conditions. Likewise, while the zonal wind of the PFJ has a strong positive correlation to the AAO, the zonal wind of the STJ has a moderate negative correlation to the AAO, thus the AAO is only weakly correlated to the SFI.

The development of the SFI also allowed for the creation of composite maps of split-flow and non-split-flow regimes. An examination of the difference in the thermal structure of the two regimes revealed a dramatic change in the strength of the temperature gradient near 60°S and 180°W. The change in the temperature gradient in the 1000–400-hPa layer between the two flow regimes was approximately 5×10^{-6} °C m^{-1} [5°C (1000 km)$^{-1}$], nearly 2 times the magnitude of the climatological temperature gradient. The change in gradient suggests a

large difference in the strength of the PFJ using simple thermal wind arguments. The implied change in the magnitude of the shear in the troposphere is on the order of 13 m s^{-1}; considering that the strength of the PFJ in the mean is about 25.5 m s^{-1}, this represents a change of nearly 50% of the mean value. The location and orientation of the temperature anomalies for the split-flow composite, both in the vertical cross sections and the thickness fields, indicate warm air poleward of Australia and New Zealand, with the bitterly cold air confined to Antarctica. Correspondingly, during nonsplit flow the temperature gradient is reversed, leading to the hypothesis that cold surges out of Antarctica into the South Pacific lead to the dissipation of the split flow.

Cross sections revealed that periods characterized by a low SFI (strong split flow) exhibit a very strong PFJ extending into the lower troposphere near 65°S, with the 20 m s^{-1} isotach extending down to about 800 hPa. In the climatology the 20 m s^{-1} isotach barely extends below 500 hPa, and in the non-split-flow composite the 20 m s^{-1} isotach remains above 150 hPa. The structure, strength, and location of the STJ is consistent with climatology in both the split and nonsplit cases. However, in the nonsplit case, the zonal wind maximum associated with the STJ is located just poleward of its climatological and strong split-flow location. The lack of variability of the STJ, in combination with the dramatic changes observed in the strength and location of the PFJ, strongly indicates that the SFI is largely modulated by variability in the PFJ, which consists of both synoptic-scale and large-scale disturbances.

These results suggest that further research into the synoptic-scale evolution, maintenance, and dissipation of split-flow events into non-split-flow events and vice versa may lead to a better understanding of the variability of the split jet, the PFJ, and the STJ in the SH. In a forthcoming companion paper we will examine the synoptic-scale evolution of split-flow and non-split-flow events.

Acknowledgments. This paper grew out of a graduate-level synoptic-dynamic laboratory class focusing on the Southern Hemisphere. We are deeply grateful to Harry van Loon, Kingtse Mo, George Kiladis, Pedro Silva Dias, and Dayton Vincent for their comments and advice. Insightful comments and suggestions from Keith Hines and an anonymous reviewer greatly improved the article. The American Meteorological Society sponsored a travel grant to the first author for the Sixth International Conference on Southern Hemisphere Meteorology and Oceanography. We are indebted to the NOAA–CIRES Climate Diagnostics Center, Boulder, Colorado, for their Web sites online at http://www.cdc.noaa.gov/ and http://www.cdc.noaa.gov/Correlations/significance.html for images and correlation information during our research; to Nate Mantua of the Joint Institute for the Study of Atmosphere and Ocean for his PDO Web site online at http://tao.atmos.washington.edu/pdo/; and to David J. Thompson for the AAO data online at http://horizon.atmos.colostate.edu/ao/. Kerry Cook of Cornell University kindly provided the code for the computation of daily streamfunction and velocity potential. This work was sponsored under National Science Foundation Grants ATM9413012 and ATM9912075.

REFERENCES

Bromwich, D. H., and T. R. Parish, 1998: Meteorology of the Antarctic. *Meteorology of the Southern Hemisphere, Meteor. Monogr.*, No. 49, Amer. Meteor. Soc., 175–200.

Chen, B. C., S. R. Smith, and D. H. Bromwich, 1996: Evolution of the tropospheric split jet over the South Pacific Ocean during the 1986–89 ENSO cycle. *Mon. Wea. Rev.*, **124,** 1711–1731.

Hines, K. M., D. H. Bromwich, and G. J. Marshall, 2000: Artificial surface pressure trends in the NCEP–NCAR reanalysis over the Southern Ocean and Antarctica. *J. Climate,* **13,** 3940–3952.

Hurrell, J. W., 1995: Decadal trends in the North Atlantic oscillation: Regional temperatures and precipitation. *Science,* **269,** 676–679.

——, H. van Loon, and D. J. Shea, 1998: The mean state of the troposphere. *Meteorology of the Southern Hemisphere, Meteor. Monogr.*, No. 49, Amer. Meteor. Soc., 1–46.

James, I. J., 1988: On the forcing of planetary-scale Rossby waves by Antarctica. *Quart. J. Roy. Meteor. Soc.*, **114,** 619–637.

Kalnay, E., and Coauthors,1996: The NCEP/NCAR 40-Year Reanalysis Project. *Bull. Amer. Meteor. Soc.*, **77,** 437–471.

Karoly, D. J., 1989: Southern Hemisphere circulation features associated with El Niño–Southern Oscillation events. *J. Climate,* **2,** 1239–1252.

Kidson, J. W., 1999: Principal modes of Southern Hemisphere low-frequency variability obtained from NCEP–NCAR reanalyses. *J. Climate,* **12,** 2808–2830.

——, and M. R. Sinclair, 1995: The influence of persistent anomalies on Southern Hemisphere storm tracks. *J. Climate,* **8,** 1938–1950.

Kistler, R., and Coauthors, 2001: The NCEP–NCAR 50-Year Reanalysis: Monthly means CD-ROM and documentation. *Bull. Amer. Meteor. Soc.*, **82,** 247–268.

Koch, S. E., M. DesJardins, and P. J. Kocin, 1983: An interactive Barnes objective map analysis scheme for use with satellite and conventional data. *J. Climate Appl. Meteor.*, **22,** 1487–1503.

Mantua, N. J., S. R. Hare, Y. Zhang, J. M. Wallace, and R. C. Francis, 1997: A Pacific interdecadal climate oscillation with impacts on salmon production. *Bull. Amer. Meteor. Soc.*, **78,** 1069–1079.

Marques, R. F., and V. B. Rao, 1999: A diagnosis of a long-lasting blocking event over the southeast Pacific Ocean. *Mon. Wea. Rev.*, **127,** 1761–1776.

Mechoso, C. R., A. O'Neill, V. D. Pope, and J. D. Farrara, 1988: A study of the stratospheric final warming of 1982 in the Southern Hemisphere. *Quart. J. Roy. Meteor. Soc.*, **114,** 1365–1384.

Mo, K. C., J. Pfaendtner, and E. Kalnay, 1987: A GCM study on the maintenance of the June 1982 blocking in the Southern Hemisphere. *J. Atmos. Sci.*, **44,** 1123–1142.

Newton, C. W., 1972: Southern Hemisphere general circulation in relation to global energy and momentum balance requirements. *Meteorology of the Southern Hemisphere, Meteor. Monogr.*, No. 35, Amer. Meteor. Soc., 215–240.

Panofsky, H. A., and G. W. Brier, 1958: *Some Applications of Statistics to Meteorology.* Pennsylvania State University, 224 pp.

Powell, F. C., 1982: *Statistical Tables for the Social, Biological and Physical Sciences.* Cambridge University Press, 96 pp.

Renwick, J. A., and M. J. Revell, 1999: Blocking over the South Pacific and Rossby wave propagation. *Mon. Wea. Rev.*, **127,** 2233–2247.

Taljaard, J. J., 1972: Synoptic meteorology of the Southern Hemisphere. *Meteorology of the Southern Hemisphere, Meteor. Monogr.*, No. 35, Amer. Meteor. Soc., 139–211.

Thompson, D. W., and J. M. Wallace, 2000: Annular modes in the

extratropical circulation. Part I: Month-to-month variability. *J. Climate,* **13,** 1000–1016.

Trenberth, K. E., 1986a: The signature of a blocking episode on the general circulation in the Southern Hemisphere. *J. Atmos. Sci.,* **43,** 2061–2069.

——, 1986b: An assessment of the impact of transient eddies on the zonal flow during a blocking episode using Eliassen–Palm flux diagnostics. *J. Atmos. Sci.,* **43,** 2070–2087.

——, 1991: Storm tracks in the Southern Hemisphere. *J. Atmos. Sci.,* **48,** 2159–2178.

——, and K. C. Mo, 1985: Blocking in the Southern Hemisphere. *Mon. Wea. Rev.,* **113,** 3–21.

van Heerden, J., and J. J. Taljaard, 1998: Africa and surrounding waters. *Meteorology of the Southern Hemisphere, Meteor. Monogr.*, No. 49, Amer. Meteor. Soc., 141–174.

van Loon, H., 1956: Blocking action in the Southern Hemisphere. *Notos,* **5,** 171–177.

——, 1972a: Temperature in the Southern Hemisphere. *Meteorology of the Southern Hemisphere, Meteor. Monogr.*, No. 35, Amer. Meteor. Soc., 9–22.

——, 1972b: Pressure in the Southern Hemisphere. *Meteorology of the Southern Hemisphere, Meteor. Monogr.*, No. 35, Amer. Meteor. Soc., 59–86.

——, 1972c: Wind in the Southern Hemisphere. *Meteorology of the Southern Hemisphere, Meteor. Monogr.*, No. 35, Amer. Meteor. Soc., 87–99.

Vincent, D. G., 1994: The South Pacific convergence zone (SPCZ): A review. *Mon. Wea. Rev.,* **122,** 1949–1970.

——, and P. L. Silva Dias, 1998: Pacific Ocean. *Meteorology of the Southern Hemisphere, Meteor. Monogr.*, No. 49, Amer. Meteor. Soc., 101–117.

——, K.-C. Ko, and J. M. Schrage, 1997: Subtropical jet streaks over the South Pacific. *Mon. Wea. Rev.,* **125,** 438–446.

Wilks, D. S., 1995: *Statistical Methods in Atmospheric Sciences—An Introduction.* Academic Press, 467 pp.